博士論文

論文題目

The role of the homeobox gene Dlx5 in craniofacial development

(頭蓋顔面形成における Dlx5 の役割)

氏名　　清水　美希

The role of the homeobox gene Dlx5

in craniofacial development

(頭蓋顔面形成における Dlx5 の役割)

東京大学大学院医学系研究科分子細胞生物学専攻

指導教員：栗原 裕基　教授

申請者：清水 美希

Table of contents

Abstract

Establishment of animal body plan is controlled by gene regulatory networks involving homeobox-containing transcription factors. In vertebrates, the regional identity of the pharyngeal arches (PAs), well-conserved segmental structures, along the anteroposterior and dorsoventral axes are determined by *Hox* and *Dlx* homeobox gene codes, respectively. However, it is unknown whether Dlx5 is sufficient for determination of the ventral identity of anterior PAs along the dorsoventral axis. Also, the molecular mechanisms whereby these homeobox genes direct region-specific genetic programs cooperatively with each other remain largely unclear. To obtain a clue to these problems, I established mice ectopically-expressing *Dlx5* in neural crest derivatives using the *Wnt1::Cre* system. Ectopic expression of *Dlx5* in the maxillary arch, the dorsal portion of the first PA (PA1), caused partial homeotic-like transformation into lower jaw-like structures, while substantial upper jaw identities still remaining in NCC-*Dlx5* mice. In addition, ectopic *Dlx5* expression in the skull caused excessive bone and cartilage formation. *In situ* hybridization and transcriptome analysis revealed that, although *Dlx5* activated a genetic cascade involved in the specification of the mandibular arch, the ventral portion of PA1, *Dlx5*-resistant maxillary-arch specific genetic program may be

operated in the maxillary arch. Transcriptome analysis further indicates that *Hoxa2* and *Dlx5* may share common downstream genes and may crosstalk to exert co-operative or competitive effects on these gene expression in a context-dependent manner. This crosstalk may contribute to the determination of regional identity and skeletogenesis in craniofacial development.

Introduction

Homeobox genes are evolutionary conserved master regulators of morphogenesis and endow the positional address to various structure (Akam, 1989; Akam, 1991; Carroll, 1995; McGinnis, W. and Krumlauf, 1992). Unveiling the functions of homeobox genes is critical to understand the basis of the animal body plan. Despite extensive studies on these genes in various species, the molecular mechanisms underlying their capacity to topologically specify the body plan remain elusive.

Pharyngeal arches (PAs) are segmental structures characteristic of the pharyngula stage of vertebrates. PAs are colonized by cranial neural crest cells (cranial NCCs, CNCCs), migratory multipotent progenitors arising from the dorsal neural tube at forebrain, midbrain and hindbrain levels, and a large part of the cranial skeletons is derived from this cell population. Identities of PAs along the dorsal-ventral (DV) and the anterior-posterior (AP) axes are defined by two different families of homeobox gene families, *Dlx* and *Hox* genes, respectively (Medeiros and Crump, 2012; Minoux and Rijli, 2010).

The maxillary process, the dorsal part of the first PA (PA1), is specified by *Dlx1*/*Dlx2*, whereas the mandibular process, the ventral part of PA1, is mainly specified by

Dlx5/*Dlx6* (Depew *et al*., 2002). Indeed, inactivation of *Dlx5* and *Dlx6* (Beverdam *et al*., 2002; Depew *et al*., 2002) or their upstream endothelin-1 (Edn1)/endothelin receptor type-A (Ednra) pathway (Kitazawa *et al*., 2015; Kurihara *et al*., 1994; Ozeki *et al*., 2004; Ruest *et al*., 2004) results in the transformation of the mandibular process into a maxillary-like one in amniote embryos. On the other hand, ectopic activation of the Edn1/Ednra signaling in the maxillary process induces up-regulation of *Dlx5*/*Dlx6* and transformation of the maxillary process into the mandibular-like one (Sato *et al*., 2008; Tavares and Clouthier, 2015), indicating that the Edn1/Ednra signaling is a molecular switch to define the jaw identity. However, whether the expression of *Dlx5* or *Dlx6* could be sufficient to cause transformation has not been examined (Fig. 1). *Dlx5* is also known as an osteogenic factor. Indeed, *Dlx5* can activate the expression of *Runx2*, which is a key regulator of osteogenesis, and promote osteogenic differentiation (Holleville *et al*., 2007; Lee *et al*., 2005).

In contrast to patterning along the DV axis, the regional identities of PAs along the AP axis are determined by the combination of *Hox* genes (Le Douarin, 2004; Minoux and Rijli, 2010). In PA1, no *Hox* genes are expressed, while the second and third PAs (PA2, PA3) are specified by *Hoxa2* (Gendron-Maguire *et al*., 1993; Rijli *et al*., 1993)

and *Hoxa3* (Chisaka and Capecchi, 1991), respectively. Inactivation of *Hoxa2* results in the homeotic transformation of PA2 into PA1-like structures (Baltzinger *et al*., 2005; Couly *et al*., 1998; Gendron-Maguire *et al*., 1993; Hunter and Prince, 2002; Rijli *et al*., 1993; Santagati *et al*., 2005). On the other hand, ectopic expression of *Hoxa2* in PA1 results in the opposite transformation into PA2-like structures (Grammatopoulos *et al*., 2000; Hunter and Prince, 2002; Kitazawa *et al*., 2015; Minoux *et al*., 2013; Pasqualetti *et al*., 2000). In PA2 and posterior PAs, *Hox* and *Dlx* genes are co-expressed in CNCCs, and might cooperate in defining craniofacial morphogenesis (Santagati and Rijli, 2003), but it remains almost unsolved whether possible crosstalk between *Hox* and *Dlx* genes contributes to the region-specific PA patterning.

To address these issues, I generated a novel mouse line that conditionally expresses *Dlx5* in the NCC population (hereafter referred to as NCC-*Dlx5* mouse). Ectopic expression of *Dlx5* in the maxillary arch cause partial homeotic-like transformation into lower jaw-like structures. Changes in gene expression profiles suggest that this transformation is incomplete because the ectopic expression of *Dlx5* alone cannot sufficiently suppress the expression of a set of maxillary process-specific genes. Interestingly, a comparison of transcriptome profiles between NCC-*Dlx5* mice and

NCC-*Hoxa2* mice (a mice line that ectopically express *Hoxa2* in the NCC-lineage (Kitazawa *et al*., 2015)), together with recent genome-wide analysis (Amin *et al*., 2015; Donaldson *et al*., 2012), reveals that *Dlx5* and *Hoxa2* share some downstream genes involved in PA development and possible regulation of the *Dlx5/6* locus by *Hoxa2*. In addition, the present study has revealed the skeletogenic activity of *Dlx5* in *in vivo* CNCCs, which is opposite to the anti-skeletogenic effect of *Hoxa2* on the same NCC population. These finding suggests that *Dlx5* may regulate different set of genes involved in the regional specification and skeletogenesis in a context-dependent manner, and contribute to craniofacial morphogenesis partly by crosstalking with *Hoxa2*.

Materials and Methods

Mice

To obtain mice carrying the *ROSA*$^{CAG\text{-}flox\text{-}Dlx5/+}$ allele, I inserted an *F3*/*FRT*-flanked cassette containing the CAG promoter, a floxed stop sequence, Flag-tagged mouse *Dlx5* cDNA and a poly(A) additional signal into the targeting vector pROSA26-1 (P. Soriano, Mount Sinai School of Medicine, New York, NY, USA) (Addgene, plasmid 21714). I performed homologous recombination on the *ROSA26* locus of B6129F1-derived ES cells. I injected targeted ES clones into ICR blastocysts to generate chimeras. Chimeras were crossbred with ICR females. *ROSA*$^{CAG\text{-}flox\text{-}Dlx5/+}$mice were crossed with *Wnt1::Cre* mice (Chai *et al*., 2000) to induce NCC-specific expression of *Dlx5* (NCC-*Dlx5* mice).

Mice carrying the *ROSA*$^{CAG\text{-}flox\text{-}Hoxa2/+}$ (Kitazawa *et al*., 2015) allele have been previously described and used in the same way to induce NCC-specific expression of *Hoxa2* (NCC-*Hoxa2* mice). The mice (*ROSA*$^{CAG\text{-}flox\text{-}Dlx5/+}$, *ROSA*$^{CAG\text{-}flox\text{-}Hoxa2/+}$, *Wnt1::Cre*, *Dlx5*/*6*-knockout) was maintained on an ICR background. Littermates without Cre-induced recombination served as controls in all experiments.

Mice were kept in an environmentally controlled room at 23±2 °C, with a relative humidity of 50–60% and under a 12-h light:12-h dark cycle. All of the animal

experiments were performed in accordance with the guidelines of the University of Tokyo Animal Care and Use Committee.

Skeletal preparation and staining

Alizarin red/ alcian blue staining was performed, as previously described (McLeod, 1980). Samples were fixed in 95% ethanol for a week, permuted to acetone for three days and incubated with 0.015% alcian blue 8GS, 0.005% alizarin red S and 5% acetic acid in 70% ethanol for three days. After washing with distilled water, the samples were cleared in 1% KOH for several days and in 1% KOH glycerol series until the surrounding tissues turned transparent. The preparations were stored in glycerol.

Histological analysis

Embryos were fixed in Bouin's solution and embedded in paraffin. The sections were subjected to Mallory trichrome stain. Three-dimensional reconstruction was performed using the Amira software (Maxnet).

***In situ* hybridization**

Whole-mount *in situ* hybridization was performed, as described previously (Wilkinson, 1992). Embryos were fixed one overnight in 4% paraformaldehyde in PBT. After dehydration and rehydration with methanol, the embryos were bleached for 1 hour in 7.5% H_2O_2 in PBT and then washed in PBT 3 times. The samples were treated with 5mg/ml proteinase K for 40 seconds at room temperature, treated with 2mg/ml glycine in PBT to stop the enzyme reaction, and post-fixed in 4% paraformaldehyde and 0.2% glutaraldehyde for 20 minutes on ice. After the pretreatment, the samples were pre-hybridized for more than 1 hour at 70°C in hybridization mix (50% formamide, 5 x SSC (1 x SSC is 0.15 M NaCl plus 0.015 M sodium citrate), 1% SDS), 50 mg/ml heparin and 50 mg/ml yeast tRNA. With digoxygenin-labeled RNA probe in hybridization mix, the samples were hybridized overnight at 70°C. The samples were then washed 3 times in hybridization mix at 70°C, then in 0.2 M NaCl, 10 mM Tris-HCl (pH7.5), 0.1% Tween-20 for 5 minutes ant treated with 100 mg/ml RNase for 30 minutes at 37°C. After a final wash in 50% formamide, 2 x SSC for 1 hour at 65°C, the samples were pre-blocked with sheep serum, incubated with alkaline

phosphatase-conjugated anti-digoxygenin antibody, and stained with nitro blue tetrazolium and 5-bromo-4-chloro-3-indoyl phosphate.

Probes for Hand2 and Goosecoid were generously provided by D. Srivastava (University of California, San Francisco, CA) and G. Yamada (Wakayama medical University, Wakayama, Japan), respectively. Other probes were prepared by RT-PCR and used in published papers (Kitazawa et al., 2015; Sato et al., 2008).

Whole mount immunostaining

Whole mount immunostaining was performed by mouse monoclonal anti-neurofilament 160 antibody (Sigma, 1:200). Signals were visualized with 3-3'-diaminobenzidine tetrahydrochloride /$NiCl_2$, as described previously (Nagy *et al*., 2003).

Quantitative real-time RT-PCR

The maxillary process, the mandibular process and the PA2 were dissected from E10.5 control and NCC-*Dlx5* mice. Total RNA was extracted from five sets of PAs by ISOGEN-II (Nippon Gene). One-μg samples were then reverse-transcribed using ReverTra Ace (TOYOBO) with RS19-15dT primer. Quantification of amount of each

mRNA was performed by real-time PCR analysis using a LightCycler (Roche) and Real-Time PCR Premix with SYBR Green (RBC Bioscience) following the manufacturer's protocol. *Glyceraldehyde-3-phosphate dehydrogenase* (*Gapdh*) was used as internal control. PCR was performed using following primers, Dlx5 previously described (Vieux-Rochas *et al*., 2010), 5′-AGACAGCCGCATCTTCT- TGT-3′ and 5′-CTTGCCGTGGGTAGAGTCAT-3′ for Gapdh.

Western blotting

The maxillary process, the mandibular process and the PA2 were dissected from E10.5 control and NCC-*Dlx5* mice. The dissected samples were lysed in lysis buffer [30 mM sodium dodecyl sulfate, 50 mM Tris/HCl (pH 7.5) and 10% (v/v) glycerol].

Transcript profiling

The maxillary process, the mandibular process and the PA2 were collected from E10.5 control and NCC-*Dlx5*. Each sample was a mixture from 3 littermates. Preparation of the cRNA and hybridization of probe array were performed on an Affymetrix GeneChip Mouse 430 2.0 array which contains 45,101 probe sets according to the manufacturer's

instructions (Affymetrix, Santa Clara, CA). The expression value for each mRNA was obtained by the Robust Multi-array Average (RMA) method. The gene set probes were filtered on an expression (20.0–100.0) percentile. Genes with the expression level lower than 20.0 percentile at least in one sample were eliminated from the analysis. After excluding the probes whose gene symbols were not identified, about 35,000 genes remained and used for further analysis. The maxillary process, the mandibular process and the PA2 were collected from E10.5 control and NCC-*Dlx5*. Preparation of the cRNA and hybridization of probe array were performed by the manufacturer's instructions (Affymetrix, Santa Clara, CA). Affymetrix GeneChip Mouse 430 2.0 array which contains 45,101 probe sets used. The expression value for each mRNA was obtained by the Robust Multi-array Average (RMA) method. The gene set probes were filtered on an expression (20.0–100.0) percentile. Genes with the expression level were lower than 20.0 percentile at least one sample were eliminated from the analysis. About 35,000 genes remained after excluding the gene set probes which did not have gene symbols. The 35,000 genes were used for further analysis. Annotation of the probe numbers and targeted sequences are shown on the Affymetrix web site.

Results

Establishment of mice ectopically expressing *Dlx5* in NCCs

To induce ectopic expression of *Dlx5* in the NCC lineage, I generated the $ROSA^{CAG\text{-}flox\text{-}Dlx5/+}$ mouse line (Fig. 2A, B), which expresses *Dlx5* in a Cre-dependent manner, and crossed it with *Wnt1::Cre* mice (Chai *et al.,* 2000). I named this line NCC-*Dlx5* (Fig. 2A). Upregulation and ectopic expression of *Dlx5* in the pharyngeal arches were ascertained by quantitative RT-PCR (Fig. 2C), Western blotting (Fig. 2D) and whole-mount *in situ* hybridization (Fig. 2E, F). I performed RT-PCR using dissected the maxillary, mandibular and second pharyngeal (PA2) arches from E10.5 control and NCC-*Dlx5* embryos. The expression level of *Dlx5* in the NCC-*Dlx5* maxillary arch was higher than the control maxillary arch and even more than control mandibular arch (Fig. 2C). Therefore, the expression level of *Dlx5* was high enough to form the maxillary into the mandibular arches as far as mRNA levels are concerned. In addition, I also confirmed the expression of introduced Flag-Dlx5 protein in the maxillary arch, mandibular arch and PA2 of E10.5 control and NCC-*Dlx5* embryos (Fig. 2D). *In situ* hybridization also showed ectopic *Dlx5* expression in cranial NCC-derivatives beyond the pharyngeal arches in consistent with the pattern of *lacZ*

expression in *Wnt-1::Cre*/*R26R* mice (Fig. 2E, F) (Jiang *et al*., 2000).

Ectopic *Dlx5* expression in NCCs causes a partial transformation of the maxillary derivatives into mandibular-like structures

The gross appearance of E18.5 NCC-*Dlx5* mice was characterized by a shortened snout, open eyelids and misaligned vibrissae (Fig. 3A-D'). Cleft palate was also observed in all 17 embryos examined at E17.5-18.5 (Fig. 3E, F). Skeletal preparations revealed malformations of the upper jaw elements. The maxilla protruded anteriorly beyond the maxilla-premaxilla suture and its zygomatic process was thick sometimes like the dentary bone (Fig. 4A-D). The jugal bone was often shortened (Fig. 4A-D) and the zygomatic and retroarticular processes of the squamosal were largely missing (Fig. 4E, F). The incus was deformed with an appearance similar to the malleus and dislocated from the stapes, which was sometimes fused to the styloid process (Fig. 4G- J). By contrast, the lower jaw elements of NCC-*Dlx5* mice were almost normal except for shortening of the coronoid process of the dentary bone (Fig. 4K, L).

In the transformed maxillary region at earlier stages, Meckel's-like rod-shaped cartilages were formed often bilaterally (Fig. 4M, N). These cartilaginous structures

were most evident at E15.5 and thereafter regressed to become undetectable at E18.5 (Fig. 5A-C). Cleft palate was associated with loss of palatine shelves formed by the processes of maxillary and palatine bones derived from the maxillary arch (Fig. 6A-D). However, another maxillary arch-derived structures such as the alisphenoid and pterygoid bones were well formed (Fig. 6A-H). Correspondingly, the maxillary arch-specific ala temporalis was normally formed separately from the Meckel's-like rod-shaped cartilage at E15.5 (Fig. 6I, J), indicating that the regional identity of the upper jaw was retained at least partially in NCC-*Dlx5* mice.

Ectopic *Dlx5* expression in NCCs affects skeletal development in the anterior neurocranium

In addition to homeotic-like transformation in the visceral skeleton, maxillary and mandibular arch-derivatives, ectopic *Dlx5* expression in NCCs caused some drastic changes in the anterior neurocranium, which is also mainly derived from NCCs (Jiang *et al.,* 2002; McBratney-Owen *et al.,* 2008). In the cranial base, the midline structures including the paranasal cartilage, presphenoid and basisphenoid of NCC-*Dlx5* mice were larger in width than those of control mice (Fig. 6E-H). In E18.5 NCC-*Dlx5* mice,

the width of the anterior edge of the basisphenoid was significantly increased compared to that of control mice (Fig. 7A-D). When the width of the parachordal plate, a mesoderm derived structure, was compared at the level of the carotid foramen between NCC-*Dlx5* and control mice at E18.5, the difference was only small, although significant (Fig. 7A-D). From the basisphenoid, ectopic cartilaginous and osseous struts extended laterally and anteriorly, respectively, the later of which fused to the hypochiasmatic cartilage, disturbing the formation of the optic foramen (Fig. 6E-J).

In the skull vault, NCCs contribute to the frontal bone, nasal bone and the central region of the interparietal bone (Jiang *et al.,* 2002). The frontal bone of E18.5 NCC-*Dlx5* mice exhibited extensive and apparently disordered ossification and chondrification, lining the region of the anterior fontanelle and displacing the parietal bone posteriorly (Fig. 8A-D). At as early as E15.5, an amorphous cartilaginous bridge was observed in the presumptive vault at the level of frontal-parietal boundary (Fig. 8E, F). These abnormalities in the neurocranium is in contrast to those of NCC-*Hoxa2* mice (Kitazawa *et al.,* 2015), which showed loss of the large part of the anterior skull vault and cartilaginous trabeculation (Fig. 8G, H), indicating that *Dlx5* might exert an effect opposite to that of Hoxa2 on skeletogenesis in the skull.

Ectopic *Dlx5*-induced skeletal defects is accompanied by soft tissue abnormalities

Maxillary-to-mandibular arch transformation in mice with ectopic activation of the Edn1/Ednra signaling was associated with misdirection of the motor root of the trigeminal nerve, which normally enters the mandibular arch and innervated the masseter (Sato *et al.,* 2008). It was divided into two symmetric branches which innervated both the mandibular and the transformed maxillary arch of ectopically Ednra-activating embryos, suggesting soft tissue transformation. To evaluate possible transformation in soft tissues of NCC-*Dlx5* embryos, we examined the morphology of cranial nerves of control and of NCC-*Dlx5* embryos at E10.5 by neurofilament immunostaining. As a result, the appearance of the trigeminal nerve branches was almost identical between control and NCC-*Dlx5* embryos, without abnormal bifurcation of the motor root of the trigeminal nerve (Fig. 9A, B). By contrast, three-dimensional reconstruction using serial sections of E17.5 control and NCC-*Dlx5* embryos revealed that the maxillary nerve, the second branch of the trigeminal nerve, of NCC-*Dlx5* mice forked into two branches, unlike its normal pattern (Fig. 9C, D; also see Fig. 4M, N). One of the branches wired along the Meckel's-like cartilage with an appearance similar to the mandibular nerve. The forked maxillary nerve might be associated with the

disturbed vibrissae which appear to segregate into two areas (Fig. 3C, D). The projection pattern of the maxillary nerve branches directed to the brainstem were unchanged (data not shown). Three-dimensional reconstruction also revealed that the stapedial artery was disappeared in association with loss of the hole in the stapes (Fig. 9C -F). In contrast to the abnormality in the trigeminal nerve, the optic nerve tract was unchanged in spite of skeletal abnormalities in the skull base with loss of the optic foramen (Fig. 9G, H).

Ectopic *Dlx5* expression upregulates ventral PA markers in the maxillary arch

The phenotypes of NCC-*Dlx5* mice suggested that the mandibular-arch specific genetic program might be operated at least partially in the maxillary arch. To test this possibility, I examined the expression pattern of several marker genes along the DV axis. *Dlx2* was expressed in both the maxillary and mandibular arches in E10.5 NCC-*Dlx5* embryos as observed in control embryos at the same stage (Fig. 10A, B). This finding also confirmed that the extent of PA regions was not affected in NCC-*Dlx5* mice. By contrast, the mandibular arch-specific *Dlx5/6*-downstream genes *Dlx3* (Fig. 10C, D), *Goosecoid* (Fig. 10E, F), *Hand2* (Fig. 10G, H) and *Pitx1* (Fig. 10I, J) were ectopically

expressed in the maxillary arch of NCC-*Dlx5* embryos, as observed in *Ednra*$^{Edn1/+}$ mice (Sato *et al*., 2008). In the PA2 of NCC-*Dlx5* embryos, *Dlx3* expression was extended dorsally, compared to control embryos (Fig. 10C, D). It is noteworthy that the upregulation of *Goosecoid* and *Pitx1* were more prominent in the maxillary arch of NCC-*Dlx5* mice than that of *Ednra*$^{Edn1/+}$ mice (Sato *et al*., 2008), indicating the mandibular (and possibly ventral PA2)-specific genetic cascade might be sufficiently activated in the maxillary arch (and possibly dorsal PA2) of NCC-*Dlx5* embryos.

Dlx5 regulates the expression of distinct sets of genes in a context-dependent manner

The results of morphological analysis and *in situ* hybridization brought to light some questions to be addressed. First, there appears to be a discrepancy between the induction of a set of *Dlx5/6*-downstream genes in the NCC-*Dlx5* maxillary arch and the fact that the *Dlx5*-induced maxillary-to-mandibular transformation was only partial with preserving some aspects of maxillary arch identity. Then, does *Dlx5* affect the expression of genes involved in maxillary arch patterning? Secondly, the skeletal phenotype of NCC-*Dlx5* may be divided into two different categories; defective

specification of the regional identity (homeotic-like transformation) and disturbed skeletogenesis. Does *Dlx5* affect different sets of genes involved in regional specification and skeletogenesis? Thirdly, previous studies in our laboratory have shown that *Dlx5/6* and *Hoxa2* may share common downstream genes revealed by luciferase assay and transcriptome analysis (Kitazawa, 2014). When the phenotypes of NCC-*Dlx5* and NCC-*Hoxa2* mice, which express each gene in the same manner, were compared, they were similar in that both genes affect mostly the maxillary arch-derivatives within the viscerocranium, but exert opposite effects on neurocranium development. What kinds of genes are regulated by both *Dlx5* and *Hoxa2*, and is there a crosstalk between these two transcription factors?

To answer these questions and further investigate mechanistic links between forced Dlx5 expression and morphological changes, we performed transcriptome analysis on PA tissues of E10.5 control and NCC-*Dlx5* embryos using the Affymetrix GeneChip system. RNA samples were separately extracted from maxillary, mandibular and hyoid (PA2) arch tissues and were subjected to microarray analysis. When the NCC-*Dlx5* maxillary arch samples were compared to those from control maxillary arches, 12 and 21 genes (14 and 25 of ~35,000 probe sets) were identified as increased or decreased by

more than 2-fold, respectively (Table 1). Scatter plot of the signal intensity showed upregulation of major mandibular marker genes previously reported to be downstream of *Dlx5/6* (Fig. 11). By contrast, maxillary marker genes reported to be upregulated in the transformed mandibular arch of *Dlx5/6*-knockout embryos showed only small deviation from the diagonal (Fig. 11).

To confirm the difference and further characterize the *Dlx5*-downstream genes, we then performed microarray analysis on PA tissues of E10.5 *Dlx5/6*-knockout embryos and compared genes changed in the transformed *Dlx5/6*-null mandibular arch to those affected in the NCC-*Dlx5* maxillary arch. As a result, 18 and 45 genes were revealed as increased or decreased by more than 2-fold, respectively (Table 2). In the genes downregulated in the *Dlx5/6*-null mandibular arch, 10 of 12 genes upregulated in the NCC-*Dlx5* maxillary arch were included (Table 2). By contrast, only 1 gene was overlapped between 18 genes upregulated in the NCC-*Dlx5* maxillary arch and 21 genes downregulated in the *Dlx5/6*-null mandibular arch (Table 2).

To characterize the genes affected in the NCC-*Dlx5* maxillary arch, we categorized expressed genes in terms of expression patterns. For this purpose, we first combined three data sets of microarray analysis for PA samples from the present NCC-*Dlx5* mice,

Dlx5/6-knockout mice and NCC-*Hoxa2* mice (ectopically expressing *Hoxa2* in all NCC derivatives) previously published in part (Kitazawa *et al*., 2015) using the RMA method. In this analysis, the numbers of genes with more than 2-fold changes in *Dlx5/6*-knockout mice and NCC-*Hoxa2* mice greatly increased compared to the original analysis (e.g. ~1,200 vs. 79 genes upregulated in the NCC-*Hoxa2* maxillary arch), although the overall trends were unchanged. Therefore, I selected genes with more than 2-fold changes in both the original and combined analysis as 'upregulated' or 'downregulated' genes for these groups. I then plotted the fold changes of the mandibular arch/PA2 and maxillary arch/PA2 signal intensities from E10.5 control samples on the abscissa and ordinate, respectively (Fig. 12). In the double logarithmic plot, genes were successfully categorized into 6 groups as indicated in the diagram (Fig. 12). The validity of this categorization was supported by previous reports and available database (*e.g*. EMAGE) showing gene expression patterns in mouse embryos. In this diagram, many of the genes upregulated in the NCC-*Dlx5* maxillary arch (Fig. 13), as well as those downregulated in the *Dlx5/6*-null mandibular arch (Fig. 14), were categorized as ventral or mandibular-predominant, whereas the downregulated genes in the NCC-*Dlx5* maxillary arch were mainly maxillary-predominant rather than common

to the dorsal PA (Fig. 13). This is in contrast to the pattern of genes upregulated in the *Dlx5/6*-null mandibular arch, which were mainly dorsal-predominant with relatively small differences in signal intensity between the maxillary arch and PA2 (Fig. 14). These results indicate that deletion of *Dlx5/6* in the mandibular arch may upregulate genes associated with the dorsal specification common to the PA1 and PA2, whereas introduction of *Dlx5* in the maxillary arch may downregulate genes rather related to maxillary-specific developmental processes.

Dlx5 shares downstream genes with _Hoxa2_

Genes upregulated or downregulated in the NCC-*Hoxa2* maxillary arch were mainly distributed along the diagonal axis, which roughly represents a PA1-PA2 (*Hox*-negative and positive) difference (Fig. 15), but many downregulated genes were categorized in Group E, where they were largely overlapped with *Dlx5*-downregulated genes (Fig. 13). Many of the genes upregulated in the *Dlx5/6*-null mandibular arch (Fig. 14) were also affected in the NCC-*Hoxa2* maxillary arch (Fig. 15). The overlapping in affected genes between the NCC-*Dlx5* and NCC-*Hoxa2* maxillary arches were further examined by categorizing genes into six groups according to differences in expression levels between

the NCC-*Dlx5* and control maxillary arches and stratifying each group into six subgroups according to differences in expression levels between the NCC-*Hoxa2* and control maxillary arches (Fig. 16). This analysis revealed that *Dlx5* and *Hoxa2* might share a significant set of downstream genes when ectopically expressed in the maxillary arch.

Genes downregulated both in the NCC-*Dlx5* and NCC-*Hoxa2* maxillary arches more than 2-folds are maxillary-predominant (Group E in Fig. 13 and Fig. 15) and enriched for neural markers, which may be related to region-specific trigeminal nerve development (Table 3). Genes upregulated both in the NCC-*Dlx5* and NCC-*Hoxa2* maxillary arches more than 2-fold include *Dlx5*/*Dlx6* and their downstream genes such as *Hand2* (Table 3), although *Dlx5* and *Dlx6* were not included in the 2-flod change group in the original microarray analysis (Table 1). On the other hand, 3 genes (*Has2*, *Dlk1* and *TBx22*) might be affected more than 2-fold in the opposite direction by ectopic *Dlx5* and *Hoxa2* expression in the maxillary arch (Table 3).

When this stratification analysis was performed on the *Dlx5*/*6*-null mandibular arch to the NCC-*Hoxa2* maxillary arch, similar correlation in fold changes were found in both direction (Fig. 17). By contrast, comparison between the NCC-*Dlx5* maxillary arch

and *Dlx5/6*-null mandibular arch revealed a significant overlapping between genes upregulated in the NCC-*Dlx5* maxillary arch and genes downregulated in the *Dlx5/6*-null mandibular arch, but genes downregulated in the NCC-*Dlx5* maxillary arch and genes upregulated in the *Dlx5/6*-null mandibular arch were largely distinct (Fig. 18).

Possible crosstalk between *Dlx5/6* and *Hoxa2*

To explore the possibility that the genes downstream of both *Dlx5* and *Hoxa2* may be direct targets of *Hoxa2* binding, I selected genes with Hoxa2-bound regions (Donaldson *et al*., 2012) from the gene sets affected in the NCC-*Dlx5* maxillary arch and performed the stratification analysis. A total of 3,316 genes (containing multiplicated ones) were extracted, among which 1 gene was upregulated and 2 genes were downregulated by more than 2 fold in the NCC-*Dlx5* maxillary arch. These 3 genes were downregulated by more than 2 fold in the NCC-*Hoxa2* maxillary arch (Table 4). Analysis for fold changes in the *Dlx5/6*-null mandibular arch displayed 16 genes upregulated and 10 genes downregulated by more than 2 fold, among which 13 and 8 genes were upregulated or downregulated by ectopic *Hoxa2* in the maxillary arch (Table 4). These

results support the possibility that *Dlx5* and *Hoxa2* may share common downstream genes.

Discussion

Regional identities of the PAs and patterning of their derivatives along the DV and AP axes are governed by *Dlx* and *Hox* genes, respectively (Medeiros and Crump, 2012; Minoux and Rijli, 2010). In particular, the two *Dlx* paralog members *Dlx5* and *Dlx6*, which are induced by the Edn1/Ednra signaling as downstream targets, determine the identities of ventral PA derivatives including the lower jaw (Beverdam *et al.,* 2002; Depew *et al.,* 2002; Ruest *et al.,* 2004; Ozeki *et al.,* 2004). In this study, I have established a mouse line in which *Dlx5* is forcibly expressed in whole NCC derivatives to elucidate whether *Dlx5* is sufficient for regional specification along the DV axis. In the viewpoint of spatiotemporal expression, *Dlx5* is normally expressed from E7.5 to E13.0 in craniofacial regions including the dorsal PAs (Bally-Cuif et al., 1992; Danielian et al., 1998). On the other hand, ectopic *Dlx5* expression in NCC-*Dlx5* mice depends of the Cre activity reflecting the expression of *Wnt1*, which first appears around E7.5 in the dorsal neural tube (Acampora et al., 1999). Consequently, it should be noted that the timing of the ectopic *Dlx5* expression in NCC-*Dlx5* mice is likely to be different from its authentic expression in wild-type mice. The present results indicate that *Dlx5* is necessary for ventral PA patterning, but appears to be insufficient to confer

a ventral identity to dorsal PA structures. Although NCC-*Dlx5* mice exhibit significant transformation of the upper jaw components into lower jaw-like structures, substantial upper jaw identities still remain in NCC-*Dlx5* mice (Fig. 19), in contrast to *Edn1*-knockin (ectopically Ednra activating) mice, in which the upper jaw skeletons are almost totally ventralized (Sato *et al*., 2008). Some possible explanations for the partial transformation in NCC-*Dlx5* mice are discussed below.

In addition, NCC-*Dlx5* mice exhibited extensive osteogenic and chondrogenic abnormalities in the anterior region of the skull, where NCCs mainly contribute to the skeletal tissues (Jiang *et al*., 2002). This finding is consistent with the previous finding that *Dlx5* activates the expression of *Runx2,* which is a key regulator of osteogenesis, and promotes osteogenic differentiation (Holleville *et al*., 2007; Lee *et al*., 2005). Thus, ectopic *Dlx5* introduction can produce two distinct phenotypes, regional specification and skeletogenesis, in different craniofacial structures derived from NCCs,

Dlx5 and morphogenetic program in craniofacial development

The upper jaw skeletons of NCC-*Dlx5* mice exhibited a mixture of maxillary and mandibular morphology. Approximately two-thirds of genes upregulated by more than

2-fold in the NCC-*Dlx5* maxillary arch were downregulated in the *Dlx5/6*-null mandibular arch by more than 1.5-fold. This gene set includes *Dlx5*, its *cis*-paralogous gene *Dlx6* and their downstream genes, which is consistent with partial maxillary-to-mandibular transformation of the NCC-*Dlx5* maxillary arch. In particular, *Hand2*, a basic-helix-loop-helix transcription factor, can induce partial maxillary-to-mandibular transformation as seen in the NCC-*Dlx5* mice, when expressed ectopically in the maxillary arch (Sato *et al*., 2008). Some morphological features such as protrusion of the maxilla anteriorly beyond the maxilla-premaxilla suture, thickened zygomatic process and defective palatine shelves are very similar between NCC-*Dlx5* mice and *Hand2* misexpressing mice, indicating that the *Dlx5-Hand2* pathway is likely to be responsible for the partial maxillary-to-mandibular transformation. In addition, upregulation of both *Dlx5* and *Dlx6* indicates a positive feedback mechanism in the transcriptional regulation of the *Dlx5/6* locus. This may form a feedback loop to facilitate the ectopic activation of the mandibular-specific genetic program.

In addition to the upregulation of lower jaw-specific genes in the maxillary arch, ectopic *Dlx5* expression did not suppress the expression of upper jaw-specific genes enough for complete lower jaw-like transformation. Previous studies have revealed that

the Edn1/Ednra-Dlx5/6 pathway and Notch-dependent pathway drive genetic programs of lower and upper jaw morphogenesis, respectively, and the two pathways antagonize to each other (Zuniga *et al*., 2010). In this context, the forced expression of *Dlx5* in the upper jaw NCC may result in the activation of the lower jaw-specific genetic program, whereas it could not suppress the upper jaw-specific one. It might be possible that *Dlx5* expression levels were not enough for the suppression of the upper jaw-specific genes. However, quantitative RT-PCR revealed the expression level of *Dlx5* in the maxillary arch of NCC-*Dlx5* embryos equivalent to the basal *Dlx5* expression level in the mandibular arch, suggesting other explanations. Another possibility is that cooperative expression of *Dlx6* may be necessary for this suppression. The structures and transcriptional activities of *Dlx5* and *Dlx6* are very similar and their roles in PA morphogenesis are largely redundant (Jeong *et al*., 2008). However, the functional difference between *Dlx5* and *Dlx6* is not thoroughly investigated. Further experiments to introduce both genes at high expression levels are required to test these possibilities.

Another important possibility is that the upper jaw-specific genetic program may be activated by tissues juxtaposed to the NCC-derived upper jaw mesenchyme. In zebrafish, ectoderm-derived BMP and its antagonistic signaling act cooperatively with

Edn signaling to determine the identities of the ventral (lower jaw) and intermediate (jaw joint) regions (Alexander *et al.,* 2011; Zuniga *et al.,* 2011). Similarly, the maxillary epithelium may confer the regional identity to NCCs and the signal may be responsible for the upper jaw genetic program, which can be antagonized by the Edn1/Ednra signaling, but not by its downstream transcription factor Dlx5.

The *Dlx5/6*-null mandibular arch appears maxillary-like transformation (Beverdam *et al.,* 2002; Depew *et al.,* 2002). By comparing gene expression profiles between control and *Dlx5/6*-null mandibular arches, previously identified *Dlx5/6*-downstream genes downregulated or upregulated in the mutant. Upregulated genes, which are selectively expressed in the maxillary but not mandibular arch, include *Pou3f3*, a gene essential for formation of some of the maxillary arch-derived skeleton (Jeong *et al.,* 2008). The present study has confirmed their findings to identify a set of genes upregulated in the *Dlx5/6*-null mandibular arch. Unexpectedly, the majority of these genes are not largely affected by *Dlx5* introduction in the maxillary arch. This may explain in part why the maxillary arch character was relatively preserved while mandibular arch-specific genetic program was activated and morphological transformation was resulted though it was incomplete. In the dorsal region of PA1, *Dlx5* may not be sufficient for overwriting

the mandibular program because of region-specific signals to establish maxillary identity.

In contrast to genes upregulated in the NCC-*Dlx5* maxillary arch, downregulated genes are largely distinct from a set of genes upregulated in the *Dlx5/6*-null mandibular arch. Many of these genes are also downregulated in the NCC-*Hoxa2* maxillary arches, suggesting a common mechanism may underlie the repression of these genes. Notably, some of the commonly downregulated genes were included in the list of genes containing Hoxa2-bound regions (Donaldson *et al.,* 2012), suggesting a possibility that Hoxa2 and Dlx5 may share a common transcriptional co-repressor. In addition, Hoxa2 may be recruited to its binding sites in the *Dlx5/6* locus and upregulate their expression when ectopically expressed in the maxillary arch, which may partly contribute to the changes in gene expression in the same direction.

Many of these genes were related to neural development. Although the trigeminal nerve innervating the PA1 was morphologically unaffected at E10.5, some developmental abnormalities might be concealed. Indeed, the NCC-*Dlx5* maxillary arch exhibited mal-alignment of the vibrissae, which is innervated be the maxillary branch of the trigeminal nerve. Abnormalities in the process of neural development related to the

affected genes may underlie the disturbed vibrissae alignment.

Possible crosstalk between *Hox* and *Dlx* genes in craniofacial morphogenesis

In the PA2, *Hox* and *Dlx* genes are co-expressed along the AP and DV axis, respectively (Depew *et al.,* 2002; Medeiros and Crump, 2012; Minoux and Rijli, 2010), and it has been of interest how they simultaneously endow CNCCs with positional information (Santagati and Rijli, 2003). Previous studies in our laboratory have shown that ectopic expression of *Hox* genes in CNCCs causes hypoplastic phenotype of craniofacial skeleton, whose severity appears to be inversely correlated with the level of *Dlx* expression in CNCCs (Kitazawa *et al.,* 2015). Knock-down of the Edn1-Dlx5/6 pathway in PAs enhanced the hypoplastic phenotype, indicating that *Dlx5* and *Dlx6* are likely to act preventing the effects of ectopic *Hox*a2 expression. In the present study, ectopic *Dlx5* expression can induce skeletogenic phenotype opposite to that of *Hoxa2* expression in the NCC-derived skull bones and cartilages. In these tissues, *Hoxa2* and *Dlx5* may affect skeletogenic programs in the opposite direction.

Transcriptome analysis in this study provides some evidence supporting a possible crosstalk between *Dlx5* and *Hoxa2*. Many genes affected in NCC-*Dlx5* or

Dlx5/6-knockout mice are also affected in NCC-*Hoxa2* mice. Previous study revealed that *Hox* and *Dlx* are homeodomain-containing transcription factors which recognize very similar sequences with a TAAT motif *in vivo* (Noyes *et al*., 2008). It is conceivable that *Hox* and *Dlx* genes may recognize common target genes and regulate them in the same or opposite direction, resulting in a complex and dynamic crosstalk. Indeed, this hypothesis is consistent with our recent data of reporter assay using culture cells, which showed competition between *Hoxa2* and *Dlx* members in TAAT-containing enhancer activity (Kitazawa, 2014). These present and previous findings suggest that *Hoxa2* and *Dlx5* may share common downstream genes. Indeed, some mandibular arch-specific genes, many of which are also expressed in the PA2, were also upregulated in the NCC-*Hoxa2* maxillary arch. In normal PA development, *Hoxa2* and *Dlx5/6* may co-operatively regulate the ventral arch-specific genetic cascade.

Furthermore, *Dlx* genes were also shown to be upregulated by *Hoxa2*. Previous reports have identified *Dlx6os1*, an antisense long non-coding RNA in the *Dlx5* locus, as a gene downregulated in the *Hoxa2*-null PA2 containing *Hoxa2*-bound regions (Donaldson *et al*., 2012) and *Dlx6* as a gene containing *Hoxa2-Meis* synergistic binding regions critical for *Hoxa2* transcriptional activity and PA morphogenesis (Amin *et al*.,

2015). This *Hoxa2-Dlx5/6* regulatory axis may also be involved in normal morphogenesis of the ventral PA2, where *Hoxa2* and *Dlx5/6* are co-expressed.

Conclusion

The present study has revealed the region-specifying and skeletogenic activity of *Dlx5* through the induction of distinct set of genes. In the maxillary arch, however, the *Dlx5*-driven mandibular arch-specific gene induction is not sufficient for complete transformation into a mandibular-like morphology. *Dlx5*-resistant maxillary-arch specific program may be operated in CNCCs contributing to the maxillary arch. The present study also indicates a possible crosstalk between *Hoxa2* and *Dlx5* in the PA2, where both genes are co-expressed. Future studies on the transcriptional activity of *Dlx5* and its own expression will advance the understanding of the molecular mechanisms underlying craniofacial development.

Acknowledgements

I thank H. Kurihara, T. Kitazawa, Y. Kawamura, Y. Wada , Y. Uchijima, Y. Kurihara, K. Tonami, R. Asai, Y. Arima, K. Fujisawa, K. Nishiyama, T. Sato, N. Takubo, D. Seya, W. Isono, K. Maruyama, S. Masuda and T. Miyake (The University of Tokyo, Tokyo, Japan) for experimental support; G. Levi and N. Narboux-Nême (Muséum National d'Histoire Naturelle, Paris, France) for analysis of mutant mice; M. Kobayashi and A. Taguchi (The University of Tokyo, Tokyo, Japan) for microarray usage; R. Mizutani and N. Akimitsu (The University of Tokyo, Tokyo, Japan) for microarray analysis.

M. Shimizu graduated a Graduate Program for Leaders in Life Innovation.

This work was supported by Graduate Program for Leaders in Life Innovation, The University of Tokyo Life Innovation Leading Graduate School from MEXT, Japan.

References

Acampora, D., Merlo, G. R., Paleari, L., Zerega, B., Postiglione, M. P., Mantero, S., Bober, E., Barbieri, O., Simeone, A. and Levi, G. (1999). Craniofacial, vestibular and bone defects in mice lacking the Distal-less-related gene Dlx5. *Development* **126**, 3795–3809.

Akam, M. (1989). Hox and HOM: homologous gene clusters in insects and vertebrates. *Cell* **57**, 347–349.

Akam, M. (1991). Developmental biology. Wondrous transformation. *Nature* **349**,.

Alexander, C., Zuniga, E., Blitz, I. L., Wada, N., Le Pabic, P., Javidan, Y., Zhang, T., Cho, K. W., Crump, J. G. and Schilling, T. F. (2011). Combinatorial roles for BMPs and Endothelin 1 in patterning the dorsal-ventral axis of the craniofacial skeleton. *Development* **138**, 5135–5146.

Amin, S., Donaldson, I. J., Zannino, D. a, Hensman, J., Rattray, M., Losa, M., Spitz, F., Ladam, F., Sagerström, C. and Bobola, N. (2015). Hoxa2 selectively enhances Meis binding to change a branchial arch ground state. *Dev. Cell* **32**, 265–77.

Bally-Cuif, L., Alvarado-Mallart, R. M., Darnell, D. K. and Wassef, M. (1992).

Relationship between Wnt-1 and En-2 expression domains during early development of normal and ectopic met-mesencephalon. *Development* **115**, 999–1009.

Baltzinger, M., Ori, M., Pasqualetti, M., Nardi, I. and Rijli, F. M. (2005). Hoxa2 knockdown in Xenopus results in hyoid to mandibular homeosis. *Dev. Dyn.* **234**, 858–67.

Beverdam, A., Merlo, G. R., Paleari, L., Mantero, S., Genova, F., Barbieri, O., Janvier, P. and Levi, G. (2002). Jaw transformation with gain of symmetry after Dlx5/Dlx6 inactivation: mirror of the past? *Genesis* **34**, 221–7.

Carroll, S. B. (1995). Homeotic genes and the evolution of arthropods and chordates. *Nature* **376**, 479–485.

Chai, Y., Jiang, X., Ito, Y., Bringas, P., Han, J., Rowitch, D. H., Soriano, P., McMahon, A. P. and Sucov, H. M. (2000). Fate of the mammalian cranial neural crest during tooth and mandibular morphogenesis. *Development* **127**, 1671–1679.

Chisaka, O. and Capecchi, M. R. (1991). Regionally restricted developmental defects resulting from targeted disruption of the mouse homeobox gene hox-1.5. *Nature* **350**, 473–479.

Couly, G., Grapin-Botton, A., Coltey, P., Ruhin, B. and Le Douarin, N. M. (1998). Determination of the identity of the derivatives of the cephalic neural crest: incompatibility between Hox gene expression and lower jaw development. *Development* **125**, 3445–59.

Danielian, P. S., Muccino, D., Rowitch, D. H., Michael, S. K. and McMahon, a P. (1998). Modification of gene activity in mouse embryos in utero by a tamoxifen-inducible form of Cre recombinase. *Curr. Biol.* **8**, 1323–1326.

Depew, M. J., Lufkin, T. and Rubenstein, J. L. R. (2002). Specification of jaw subdivisions by Dlx genes. *Science* **298**, 381–385.

Donaldson, I. J., Amin, S., Hensman, J. J., Kutejova, E., Rattray, M., Lawrence, N., Hayes, A., Ward, C. M. and Bobola, N. (2012). Genome-wide occupancy links Hoxa2 to Wnt-β-catenin signaling in mouse embryonic development. *Nucleic Acids Res.* **40**, 3990–4001.

Gendron-Maguire, M., Mallo, M., Zhang, M. and Gridley, T. (1993). Hoxa-2 mutant mice exhibit homeotic transformation of skeletal elements derived from cranial neural crest. *Cell* **75**, 1317–1331.

Grammatopoulos, G. A., Bell, E., Toole, L., Lumsden, A. and Tucker, A. S. (2000).

Homeotic transformation of branchial arch identity after Hoxa2 overexpression. *Development* **127**, 5355–5365.

Holleville, N., Matéos, S., Bontoux, M., Bollerot, K. and Monsoro-Burq, A. (2007). Dlx5 drives Runx2 expression and osteogenic differentiation in developing cranial suture mesenchyme. *Dev. Biol.* **304**, 860–874.

Hunter, M. P. and Prince, V. E. (2002). Zebrafish hox paralogue group 2 genes function redundantly as selector genes to pattern the second pharyngeal arch. *Dev. Biol.* **247**, 367–389.

Jeong, J., Li, X., McEvilly, R. J., Rosenfeld, M. G., Lufkin, T. and Rubenstein, J. L. R. (2008). Dlx genes pattern mammalian jaw primordium by regulating both lower jaw-specific and upper jaw-specific genetic programs. *Development* **135**, 2905–2916.

Jiang, X., Rowitch, D. H., Soriano, P., McMahon, A. P. and Sucov, H. M. (2000). Fate of the mammalian cardiac neural crest. *Development* **127**, 1607–1616.

Jiang, X., Iseki, S., Maxson, R. E., Sucov, H. M. and Morriss-Kay, G. M. (2002). Tissue origins and interactions in the mammalian skull vault. *Dev. Biol.* **241**, 106–116.

Kitazawa, T. (2014). Analysis of pharyngeal arch patterning by Hox and Dlx genes: evolutionary and developmental implication for vertebrates craniofacial morphogenesis. Thesis, Graduate school of medicine, The University of Tokyo

Kitazawa, T., Fujisawa, K., Narboux-Nême, N., Arima, Y., Kawamura, Y., Inoue, T., Wada, Y., Kohro, T., Aburatani, H., Kodama, T., et al. (2015). Distinct effects of Hoxa2 overexpression in cranial neural crest populations reveal that the mammalian hyomandibular-ceratohyal boundary maps within the styloid process. *Dev. Biol.* **402**, 162–174.

Kurihara, Y., Kurihara, H., Suzuki, H., Kodama, T., Maemura, K., Nagai, R., Oda, H., Kuwaki, T., Cao, W. H. and Kamada, N. (1994). Elevated blood pressure and craniofacial abnormalities in mice deficient in endothelin-1. *Nature* **368**, 703–710.

Le Douarin, N. M. (2004). The avian embryo as a model to study the development of the neural crest: A long and still ongoing story. *Mech. Dev.* **121**, 1089–1102.

Lee, M.-H., Kim, Y.-J., Yoon, W.-J., Kim, J.-I., Kim, B.-G., Hwang, Y.-S., Wozney, J. M., Chi, X.-Z., Bae, S.-C., Choi, K.-Y., et al. (2005). Dlx5 Specifically Regulates Runx2 Type II Expression by Binding to Homeodomain-response

Elements in the Runx2 Distal Promoter. *J. Biol. Chem.* **280**, 35579–35587.

Louis-Bruno Ruest, Xilin Xiang, Kim-Chew Lim, G. L. and D. E. C. (2004). Endothelin-A receptor-dependent and -independent signaling pathways in establishing mandibular identity. *Development* **131**, 4413–4423.

McBratney-Owen, B., Iseki, S., Bamforth, S. D., Olsen, B. R. and Morriss-Kay, G. M. (2008). Development and tissue origins of the mammalian cranial base. *Dev. Biol.* **322**, 121–132.

McGinnis, W. and Krumlauf, R. (1992). Homeobox genes and axial patterning. *Cell* **68**, 283–302.

McLeod, M. J. (1980). Differential staining of cartilage and bone in whole mouse fetuses by alcian blue and alizarin red S. *Teratology* **22**, 299–301.

Medeiros, D. M. and Crump, J. G. (2012). New perspectives on pharyngeal dorsoventral patterning in development and evolution of the vertebrate jaw. *Dev. Biol.* **371**, 121–135.

Minoux, M. and Rijli, F. M. (2010). Molecular mechanisms of cranial neural crest cell migration and patterning in craniofacial development. *Development* **137**, 2605–2621.

Minoux, M., Kratochwil, C. F., Ducret, S., Amin, S., Kitazawa, T., Kurihara, H., Bobola, N., Vilain, N. and Rijli, F. M. (2013). Mouse Hoxa2 mutations provide a model for microtia and auricle duplication. *Development* **140**, 4386–97.

Nagy A., Gertsenstein M., Vintersten K., B. R. (2003). *Manipulating the Mouse Embryo: A Laboratory Manual*. 3rd ed. NY: Cold Spring Harbor Lab Press, Plainview.

Noyes, M. B., Christensen, R. G., Wakabayashi, A., Stormo, G. D., Brodsky, M. H. and Wolfe, S. a. (2008). Analysis of Homeodomain Specificities Allows the Family-wide Prediction of Preferred Recognition Sites. *Cell* **133**, 1277–1289.

Ozeki, H., Kurihara, Y., Tonami, K., Watatani, S. and Kurihara, H. (2004). Endothelin-1 regulates the dorsoventral branchial arch patterning in mice. *Mech. Dev.* **121**, 387–395.

Pasqualetti, M., Ori, M., Nardi, I. and Rijli, F. M. (2000). Ectopic Hoxa2 induction after neural crest migration results in homeosis of jaw elements in Xenopus. *Development* **127**, 5367–5378.

Rijli, F. M., Mark, M., Lakkaraju, S., Dierich, A., Dollé, P. and Chambon, P. (1993). A homeotic transformation is generated in the rostral branchial region of

the head by disruption of Hoxa-2, which acts as a selector gene. *Cell* **75**, 1333–1349.

Santagati, F. and Rijli, F. M. (2003). Cranial neural crest and the building of the vertebrate head. *Nat. Rev. Neurosci.* **4**, 806–818.

Santagati, F., Minoux, M., Ren, S.-Y. and Rijli, F. M. (2005). Temporal requirement of Hoxa2 in cranial neural crest skeletal morphogenesis. *Development* **132**, 4927–4936.

Sato, T., Kurihara, Y., Asai, R., Kawamura, Y., Tonami, K., Uchijima, Y., Heude, E., Ekker, M., Levi, G. and Kurihara, H. (2008). An endothelin-1 switch specifies maxillomandibular identity. *Proc. Natl. Acad. Sci. U. S. A.* **105**, 18806–18811.

Tavares, A. L. P. and Clouthier, D. E. (2015). Cre recombinase-regulated Endothelin1 transgenic mouse lines: Novel tools for analysis of embryonic and adult disorders. *Dev. Biol.* **400**, 191–201.

Vieux-Rochas, M., Mantero, S., Heude, E., Barbieri, O., Astigiano, S., Couly, G., Kurihara, H., Levi, G. and Merlo, G. R. (2010). Spatio-temporal dynamics of gene expression of the Edn1-Dlx5/6 pathway during development of the lower jaw.

Genesis **48**, 362–373.

Wilkinson, D. G. (1992). *In Situ Hybridization: A Practical Approach*. Oxford: IRL Press at Oxford University Press.

Zuniga, E., Stellabotte, F. and Crump, J. G. (2010). Jagged-Notch signaling ensures dorsal skeletal identity in the vertebrate face. *Development* **137**, 1843–1852.

Zuniga, E., Rippen, M., Alexander, C., Schilling, T. F. and Crump, J. G. (2011). Gremlin 2 regulates distinct roles of BMP and Endothelin 1 signaling in dorsoventral patterning of the facial skeleton. *Development* **138**, 5147–5156.

Figures and Tables

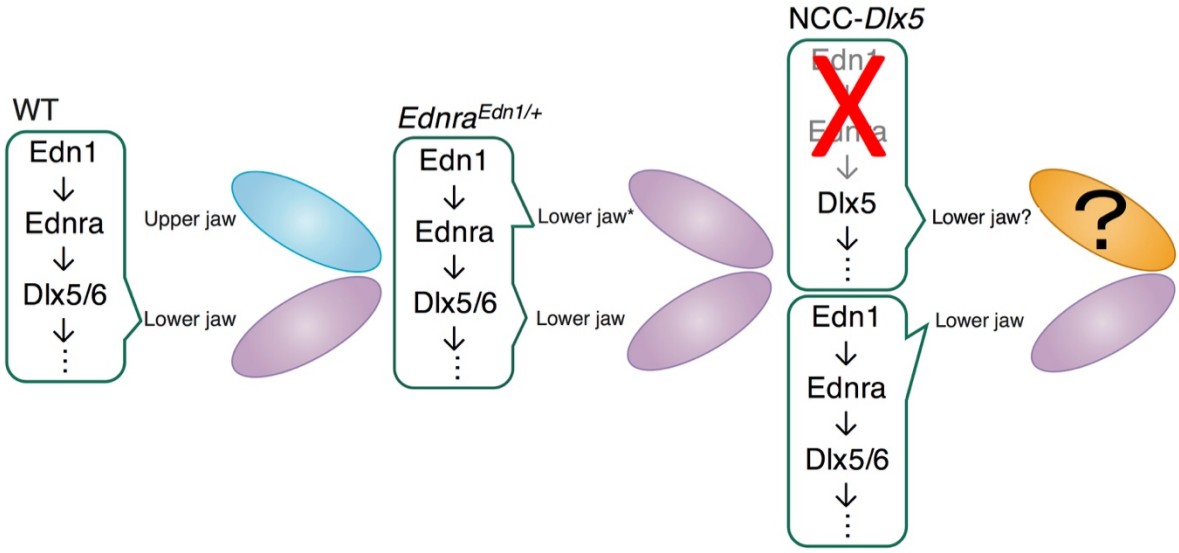

Figure 1.

A scheme illustrating regional patterning along the DV axis in wild-type, *Ednra*$^{Edn1/+}$ and NCC-*Dlx5* PA1.

The regional identities of the upper jaw (dorsal) and lower jaw (ventral) are determined by the Edn1/Ednra signaling. In wild-type mice, the Edn1/Ednra pathway induces the expression of *Dlx5/6* only in the mandibular arch to form the lower jaw. On the other hand, ectopic activation of the Edn1/Ednra pathway transforms the upper jaw into a lower jaw-like structure. In this study, I established NCC-*Dlx5* mice to examine whether ectopic *Dlx5* expression is sufficient for conferring a lower jaw identity on the upper jaw.

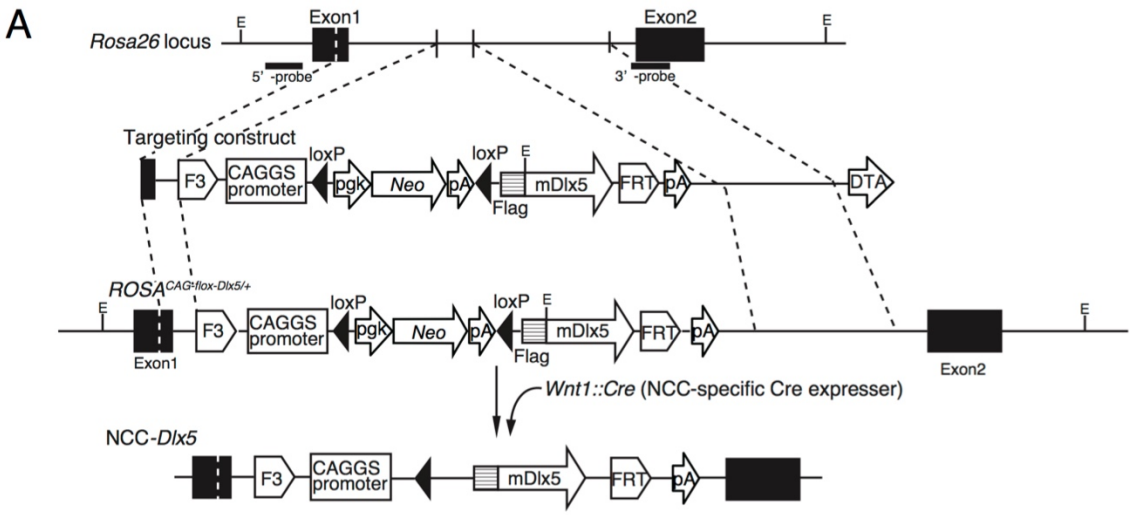
A
Rosa26 locus
E
Exon1
Exon2
5' -probe
3' -probe
Targeting construct
F3
CAGGS promoter
loxP
pgk
Neo
pA
mDlx5
Flag
FRT
DTA
ROSA CAG-flox-Dlx5/+
Wnt1::Cre (NCC-specific Cre expresser)
NCC-Dlx5

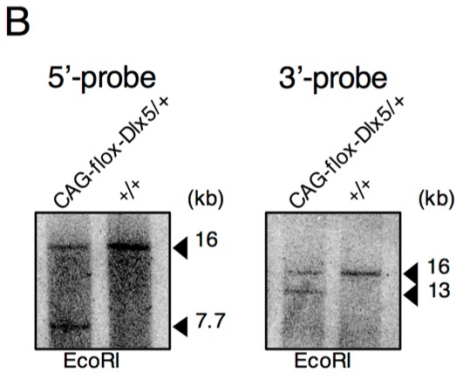
B
5'-probe
3'-probe
CAG-flox-Dlx5/+
+/+
(kb)
16
7.7
13
EcoRI

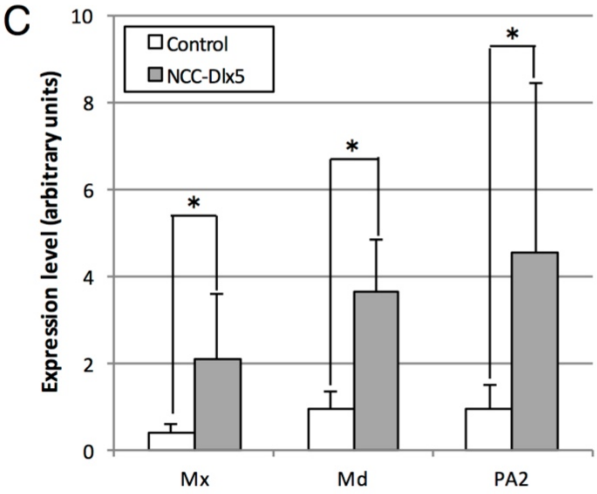
C
Control
NCC-Dlx5
Expression level (arbitrary units)
Mx
Md
PA2

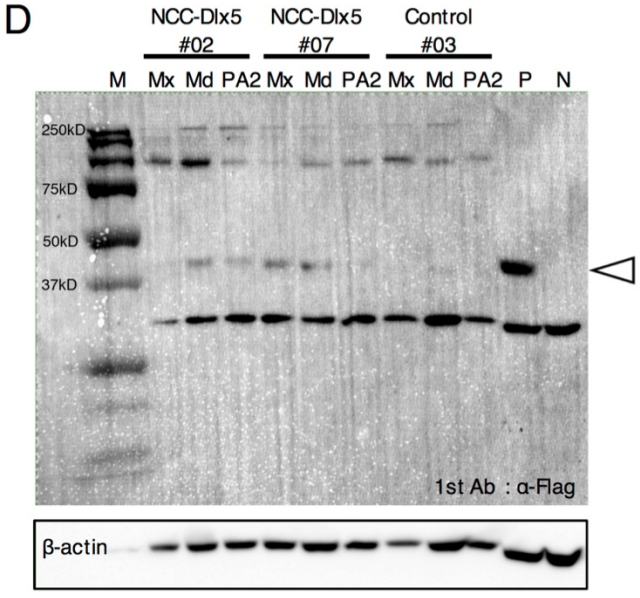
D
NCC-Dlx5 #02
NCC-Dlx5 #07
Control #03
M Mx Md PA2 Mx Md PA2 Mx Md PA2 P N
250kD
75kD
50kD
37kD
1st Ab : α-Flag
β-actin

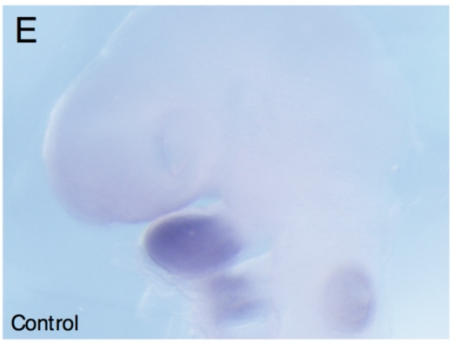
E
Control

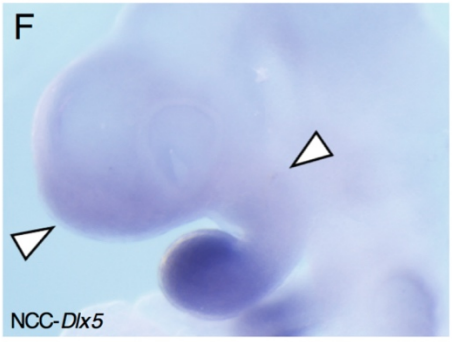
F
NCC-Dlx5

Figure 2.

Establishment of NCC-*Dlx5* mice.

(A) Strategy for conditional expression of *Dlx5* from the *Rosa26* locus and establishment of NCC-*Dlx5* mice. Probes for genotyping are indicated as 5'- and 3'-probes. E, *Eco*RI.

(B) Southern blot analysis on *Eco*RI-digested genomic DNA from ES cells used for $ROSA^{CAG\text{-}flox\text{-}Dlx5/+}$ mice.

(C) Comparison of *Dlx5* mRNA levels in the maxillary arch (Mx), mandibular arch (Md) and PA2 between control and NCC-*Dlx5* embryos at E10.5. Messenger RNA levels were estimated by quantitative RT-PCR. The values showed on the graph were mean ± SD of 5 samples (duplicated). Statistic assessments were performed by applying Mann-Whitney U test using R-software (version 3.1.3). *$p<0.01$.

(D) Western blot analysis for Flag-tagged Dlx5 protein expressed from the transgene using anti-Flag antibody. Flag-Dlx5-transfected and untransfected NIH 3T3 cell lysates serve as positive (P) and negative (N) controls, respectively.

(E and F) Whole mount *in situ* hybridization for *Dlx5* at E9.5 in control mice and NCC-*Dlx5* mice. White arrowheads indicate signals for ectopic *Dlx5* expression in CNCC-derived head and PA ectomesenchyme.

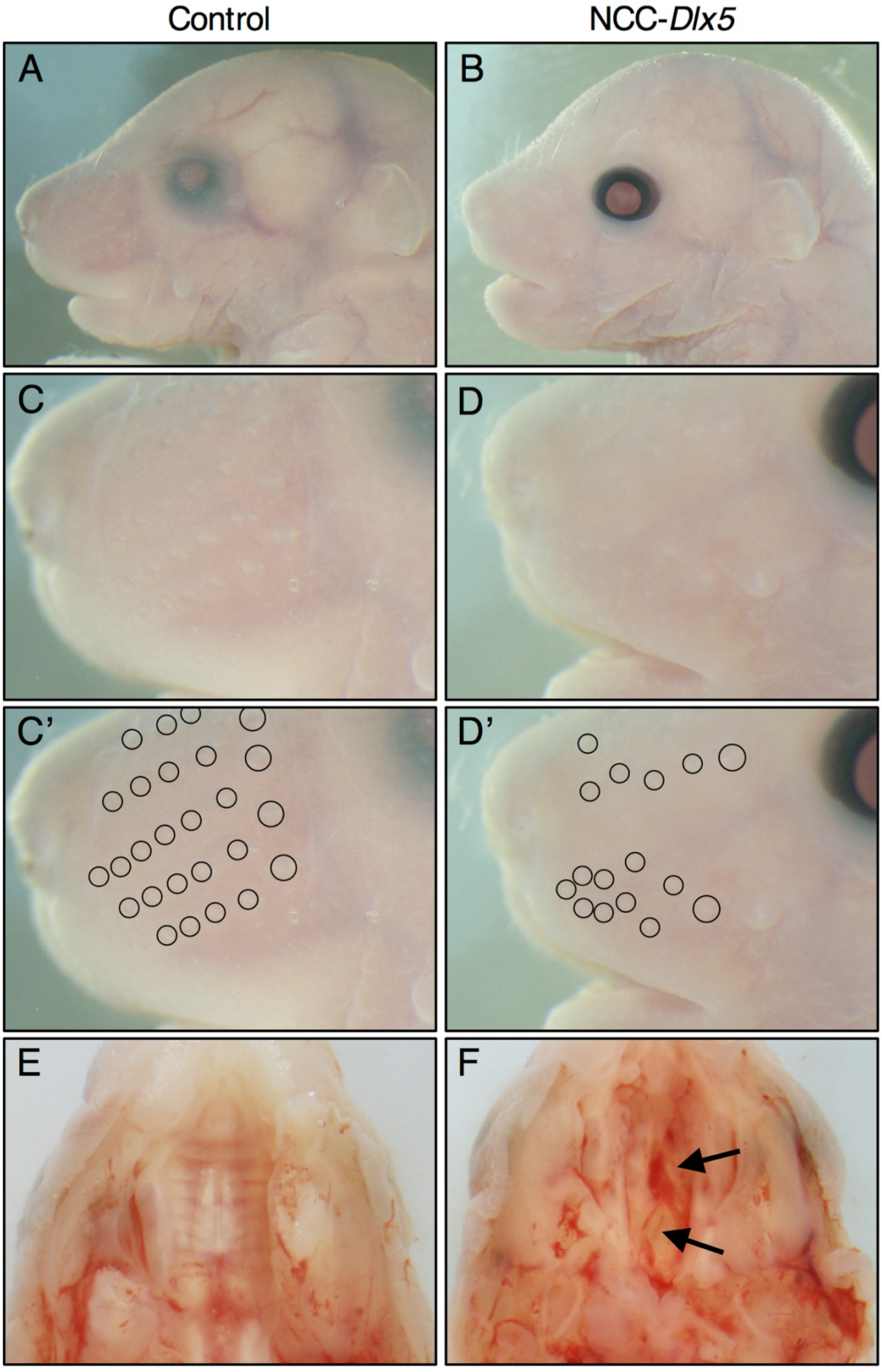
Control
NCC-Dlx5
A
B
C
D
C'
D'
E
F

Figure 3.

Gross appearance of NCC-*Dlx5* mice at E18.5.

(A, B, C and D) Facial appearance of control (A and C) and NCC-*Dlx5* (B and D) mice. NCC-*Dlx5* mice show open eyelids, shortened snout and misaligned vibrissae.

(C' and D') The vibrissae are marked by open circles.

(E and F) NCC-*Dlx5* mice exhibit cleft palate (arrows).

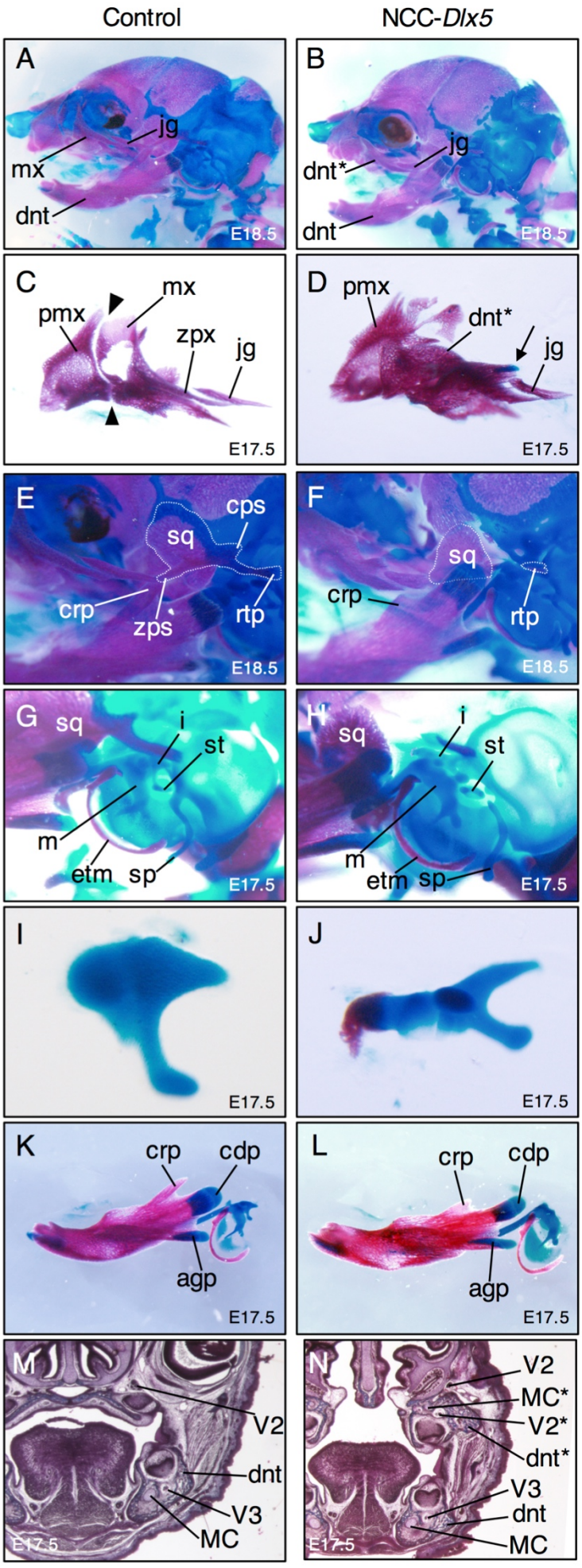
Control
NCC-Dlx5
A
jg
mx
dnt
E18.5
B
jg
dnt*
dnt
E18.5
C
mx
pmx
zpx
jg
E17.5
D
pmx
dnt*
jg
E17.5
E
cps
sq
crp
zps
rtp
E18.5
F
sq
crp
rtp
E18.5
G
sq
i
st
m
etm
sp
E17.5
H
sq
i
st
m
etm
sp
E17.5
I
E17.5
J
E17.5
K
crp
cdp
agp
E17.5
L
crp
cdp
agp
E17.5
M
V2
dnt
V3
MC
E17.5
N
V2
MC*
V2*
dnt*
V3
dnt
MC
E17.5

Figure 4.

Partial transformation of upper jaw components into lower jaw-like structures in NCC-*Dlx5* mice.

(A and B) Lateral views of E18.5 control (A) and NCC-*Dlx5* mice (B). The maxilla is deformed with dentary-like thickening of the zygomatic process and the jugal is shortened in NCC-*Dlx5* mice.

(C and D) Maxilla of E17.5 control (C) and NCC-*Dlx5* mice (D). The maxilla-premaxilla suture (between arrowheads) is hidden by the protruded maxilla and the angular process like cartilage (arrow) appears in NCC-*Dlx5* mice.

(E and F) Jaw joint region of E18.5 control (E) and NCC-*Dlx5* mice (F). The zygomatic and retroarticular processes of the squamosal are missing and the coronoid process of the dentary bone is hypoplastic in NCC-*Dlx5* mice.

(G-J) Middle ear components of E17.5 control (G. I) and NCC-*Dlx5* mice (H, J). The incus (Isolated in I and J) is deformed and dislocated from the stapes fused to the styloid process in NCC-*Dlx5* mice.

(K and L) Dentary bone of E17.5 control (K) and NCC-*Dlx5* mice (L). The coronoid process is hypoplastic in NCC-*Dlx5* mice.

(M and N) The coronal section of E17.5 control (M) and NCC-*Dlx5* mice (M). An ectopic Meckel's-like cartilage (MC*) emerges in the vicinity of the zygomatic process of the maxilla transformed into dentary-like morphology (dnt*) in the upper jaw region.

agp, angular process; cdp, condylar process; cps, caudal process of squamosal; crp, coronoid process; dnt, dentary bone; etm, ectotympanic ring; i, incus; jg, jugal bone; m, malleus; MC, Meckel's cartilage; mx, maxilla; pmx, premaxilla; rtp, retroarticular process of squamosal; sp, styloid process; sq, squamosal; st, stapes; V2, maxillary nerve; V3, mandibular nerve; zps, zygomatic process of squamosal; zpx, zygomatic process of maxilla; *, ectopic structure.

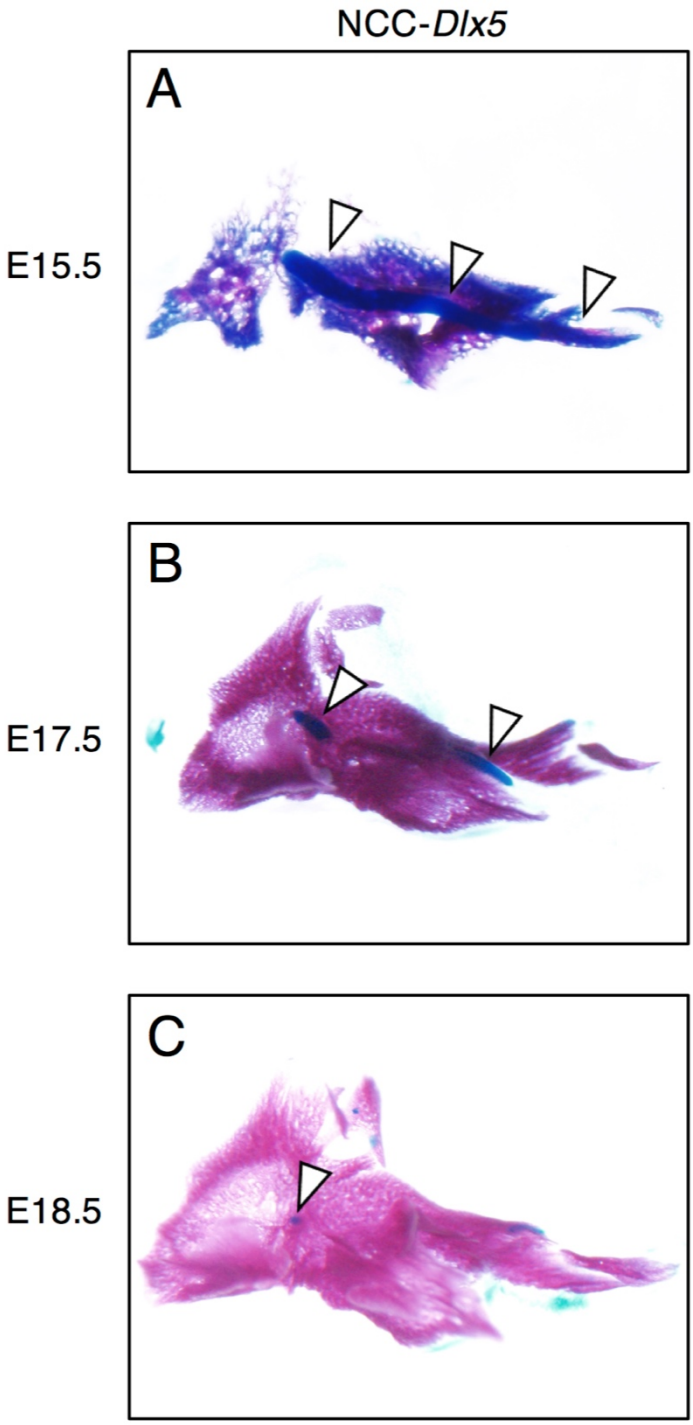

Figure 5.

Meckel's like cartilage formation in NCC-*Dlx5* mice.

(A - C) Medial views of the right maxillary components of the NCC-*Dlx5* mice. The Meckel's like cartilage is most evident at E15.5. Thereafter, this ectopic cartilage becomes gradually shortened and largely disappears (indicated by white arrowheads).

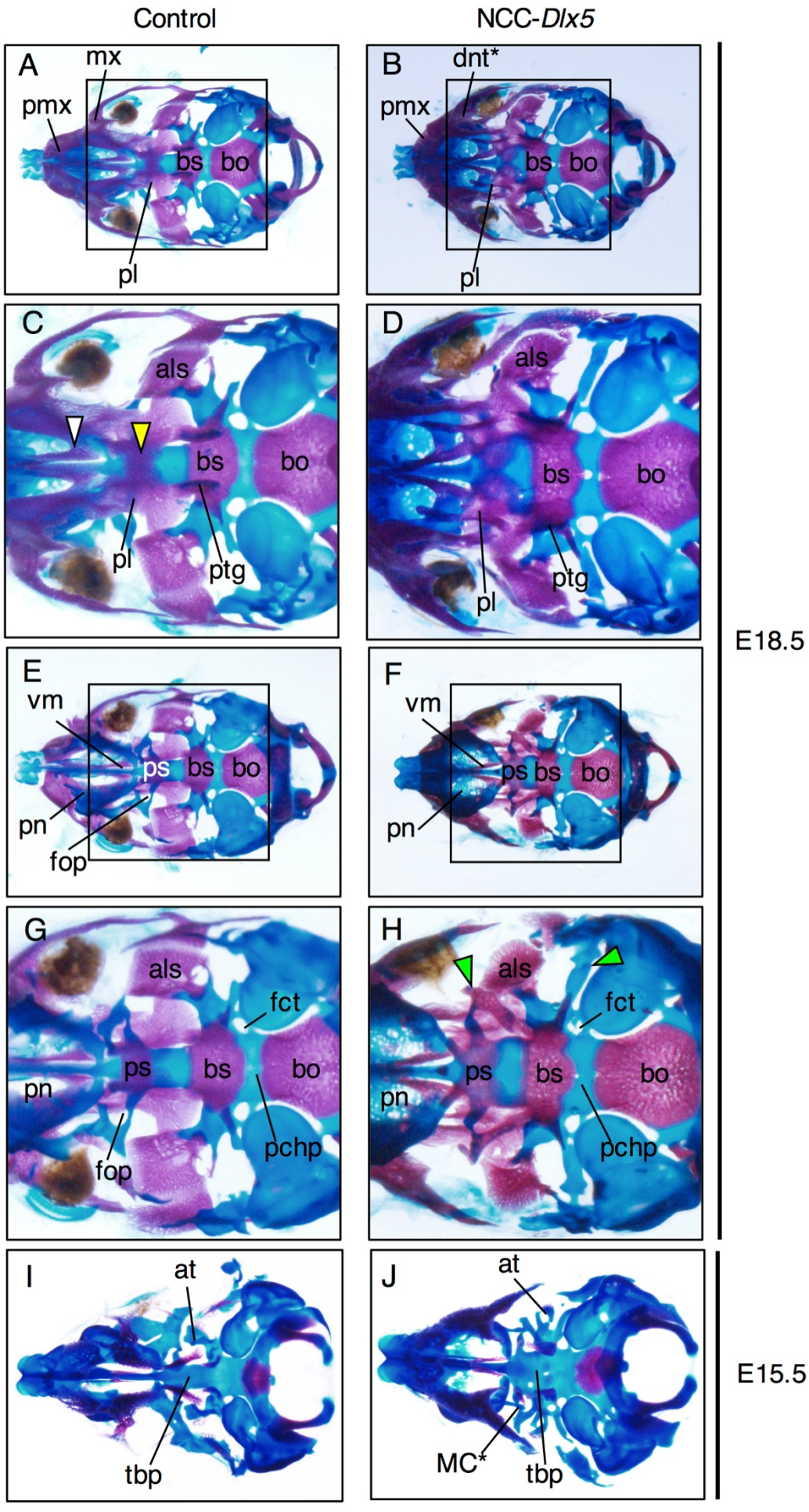
Control
NCC-*Dlx5*
A
mx
pmx
bs
bo
pl
B
dnt*
pmx
bs
bo
pl
C
als
bs
bo
pl
ptg
D
als
bs
bo
ptg
pl
E18.5
E
vm
ps
bs
bo
pn
fop
F
vm
ps
bs
bo
pn
G
als
fct
ps
bs
bo
pn
pchp
fop
H
als
fct
ps
bs
bo
pn
pchp
I
at
tbp
J
at
MC*
tbp
E15.5

Figure 6.

Cranial base deformity in NCC-*Dlx5* mice.

(A-H) Ventral (A-D) and dorsal (E-H) views of the cranial base of E18.5 control (A, C, E and G) and NCC-*Dlx5* mice (B, D, F and H). Boxed areas in A, B, E and F are magnified in C, D, G and H, respectively. In the NCC-*Dlx5* mice, palatal processes of the maxilla (white arrowhead in C) and palatine (yellow arrowhead in D) are defective (A- D). The paranasal cartilage, presphenoid and basisphenoid are enlarged in width (E-H). Ectopic cartilaginous and osseous struts extended from the basisphenoid laterally and anteriorly, respectively (green arrowheads in H).

(I and J) The ala temporalis is normally formed in E15.5 control (G) and NCC-*Dlx5* mice (H). Meckel's-like ectopic cartilage is formed separately from the ala temporalis in the NCC-*Dlx5* mice (J). Enlargement of the trabecular basal plate is evident in the NCC-*Dlx5* cranial base.

als, alisphenoidal bone; at, ala temporalis; bo, basioccipital bone; bs, basisphenoidal bone; dnt, dentary bone; fct, carotid foramen; mx, maxilla; fop, optic foramen; pchp, parachordal plate; pl, palatine; pmx, premaxilla; pn, paranasal cartilage; ps, presphenoidal bone; ptg, pterygoid; tbp, trabecular basal plate; vm, vomer; *, ectopic structure.

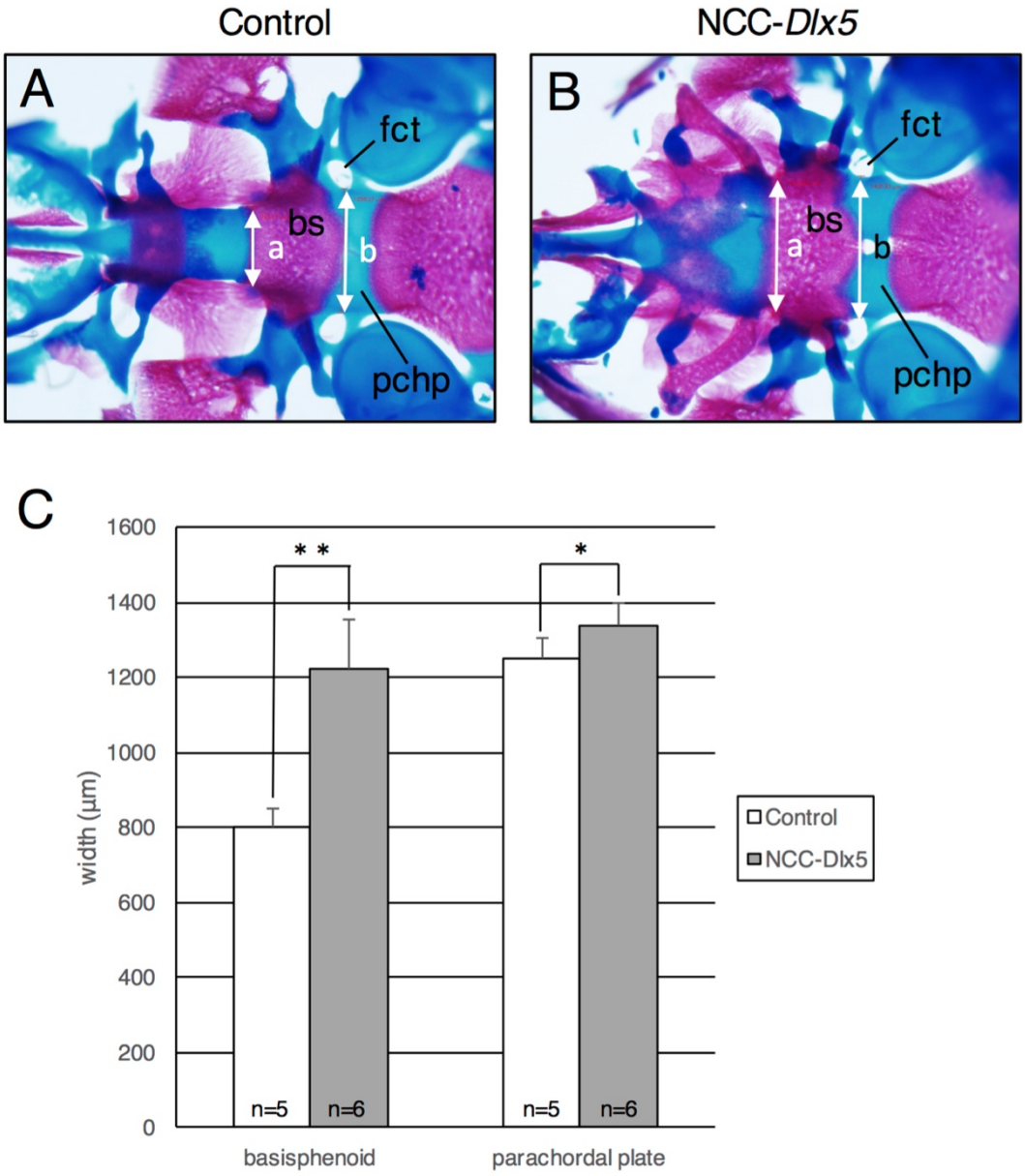

Figure 7.

Widening of the midline portion of the cranial base in NCC-*Dlx5* mice.

(A and B) Measurement of the width of the cranial base components in the midline. The width of the anterior edge of the basisphenoid (a) and that of the parachordal plate at the level of the carotid foramen (b) are measured in E18.5 control (A) and NCC-*Dlx5* mice (B). bs, basisphenoidal bone; fct, carotid foramen; pchp, parachordal plate.

(C) Comparison of the width of the basisphenoid and the parachordal plate between control (A) and NCC-*Dlx5* mice (B) at E18.5. The values showed on the graph were mean ± SD of 5 or 6 samples. Statistic assessments were performed by applying Mann-Whitney U test using R-software (version 3.1.3). *p<0.05, **p<0.01.

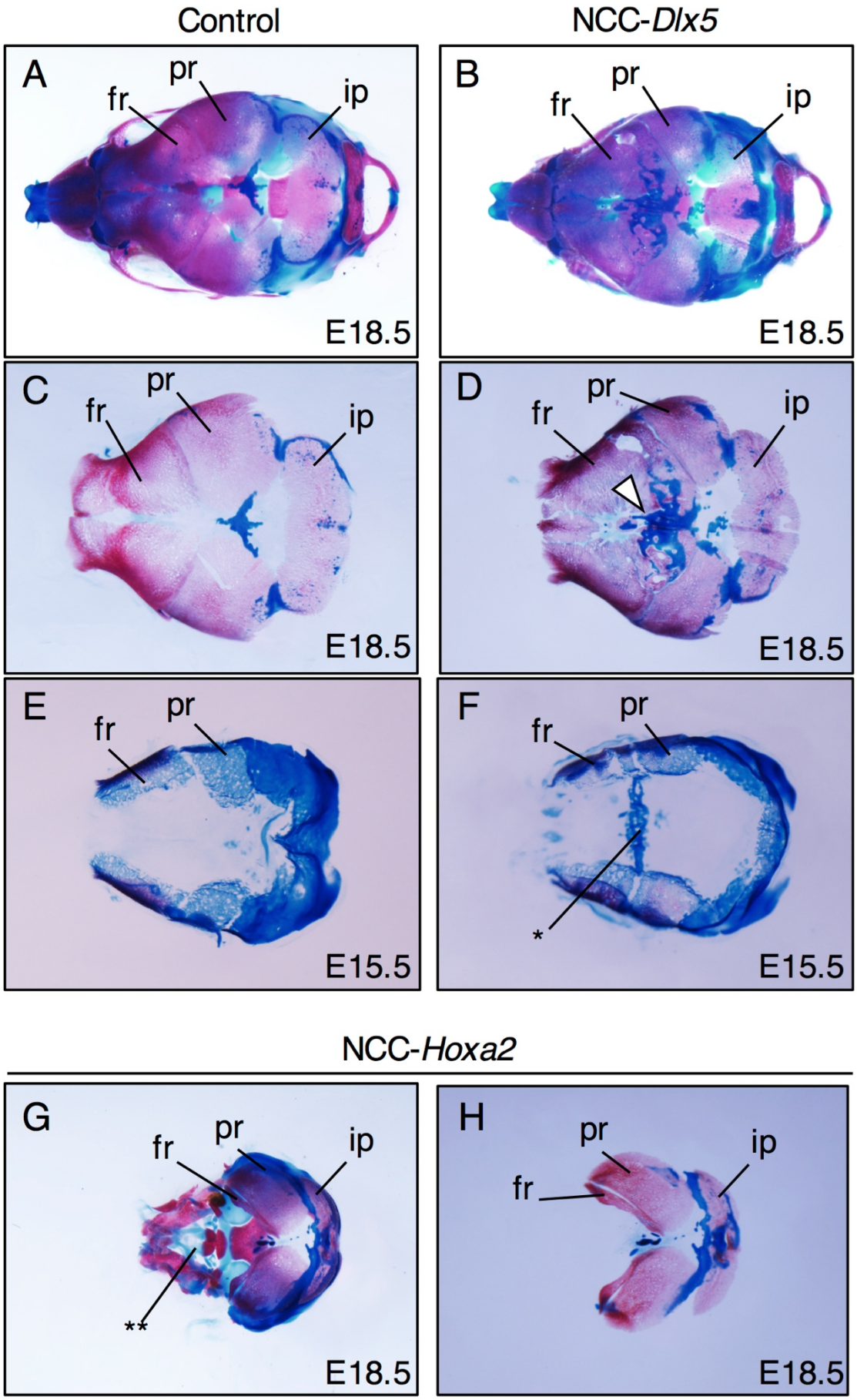
Control
NCC-*Dlx5*
A
pr
fr
ip
E18.5
B
pr
fr
ip
E18.5
C
pr
fr
ip
E18.5
D
pr
fr
ip
E18.5
E
pr
fr
E15.5
F
pr
fr
*
E15.5
NCC-*Hoxa2*
G
fr
pr
ip
**
E18.5
H
pr
ip
fr
E18.5

Figure 8.

Excessive bone and cartilage formation in the anterior skull vault of NCC-*Dlx5* mice.

(A -H) Dorsal views of the skull vault of control (A, C, E), NCC-*Dlx5* (B, D, F) and NCC-*Hoxa2* (G, H) mice at E18.5 (A-D, G, H) or E15.5 (E, F). In C-F and H, the frontal, parietal and interparietal bones are excised (with the occipital bones in E and F). The NCC-*Dlx5* frontal bone shows aberrant ossification and chondrification, extending over the region of the anterior fontanelle (white arrowhead) and displacing the parietal bone posteriorly (B, D). An amorphous cartilaginous bridge (*) is formed at the level of frontal-parietal boundary as early as E15.5 (F). The NCC-*Hoxa2* skull vault shows loss of the large part of the frontal bone and malformation of cartilaginous trabeculation (**) (G, H).

fr, frontal bone; ip, interparietal bone; pr, parietal bone.

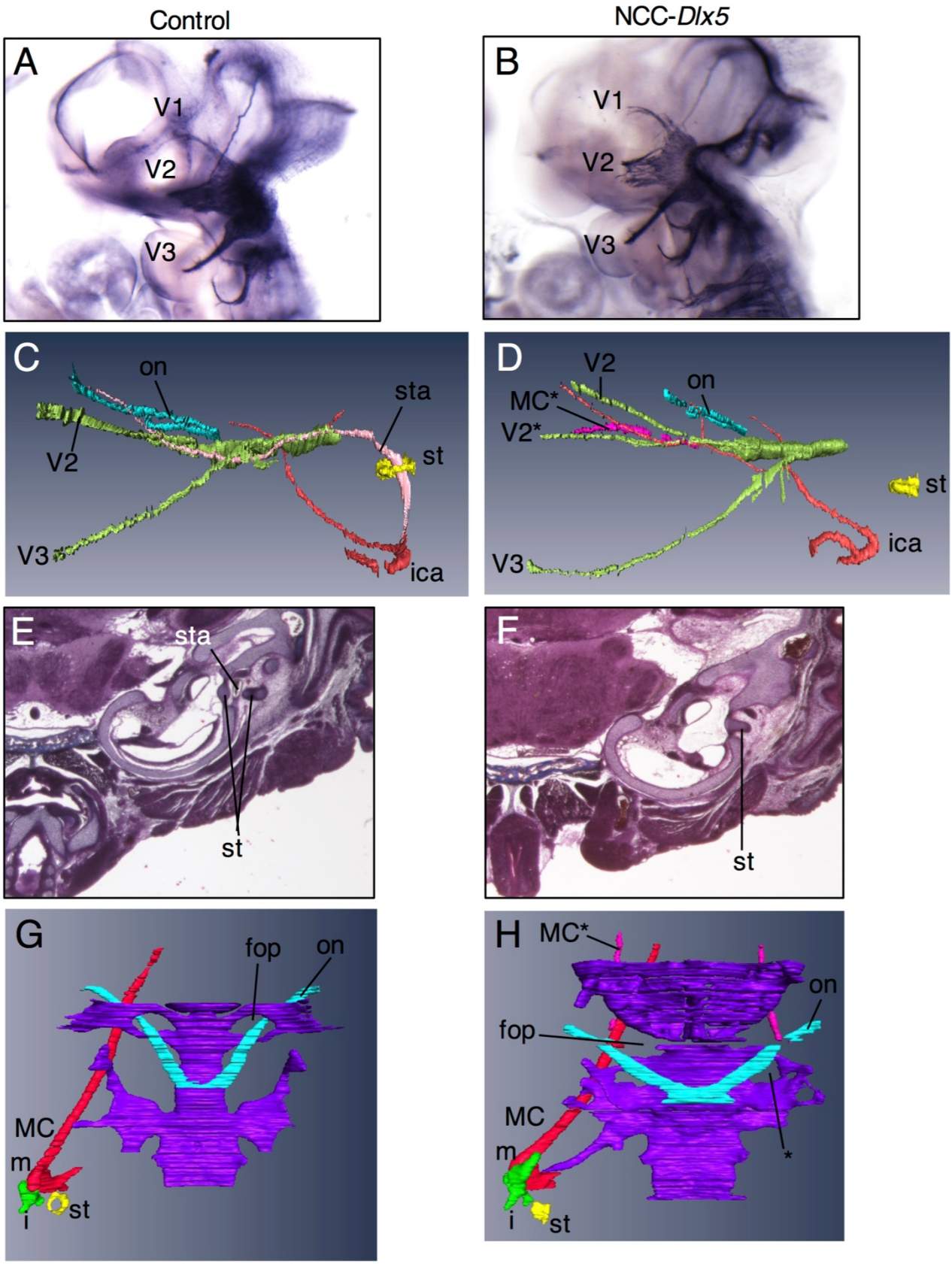
Control
NCC-Dlx5
A
V1
V2
V3
B
V1
V2
V3
C
on
sta
V2
st
V3
ica
D
V2
MC*
V2*
on
st
ica
V3
E
sta
st
F
st
G
fop
on
MC
m
i
st
H
MC*
on
fop
MC
m
*
i
st

Figure 9.

Soft tissue malformations in NCC-*Dlx5* mice.

(A and B) Cranial nerves of E10.5 control (A) and NCC-*Dlx5* mice (B) visualized by neurofilament immunostaining. No apparent differences are observed.

(C and D) 3-D reconstruction of nerves and arteries in the maxillary-mandibular region of control (C) and NCC-*Dlx5* mice (D) at E17.5. The maxillary nerve is bifurcated and the stapedial artery is not identified in NCC-*Dlx5* mice.

(E and F) The coronal section of the E17.5 control (E) and NCC-*Dlx5* (F) ear at the level of the stapes. The stapes is malformed and the stapedial artery is not observed in NCC-*Dlx5* mice.

(G and H) 3-D reconstruction showing the middle ear ossicles, Meckel's cartilage and passage of the optic nerve in control (G) and NCC-*Dlx5* mice (H) at E17.5. The optic nerve tract is unaffected by loss of the optic foramen.

fop, optic foramen; i, incus; m, malleus; ica, internal carotid artery; MC, Meckel's cartilage; on, optic nerve; st, stapes; sta, stapedial artery, V1, ophthalmic nerve; V2, maxillary nerve; V3, mandibular nerve; *, ectopic structure.

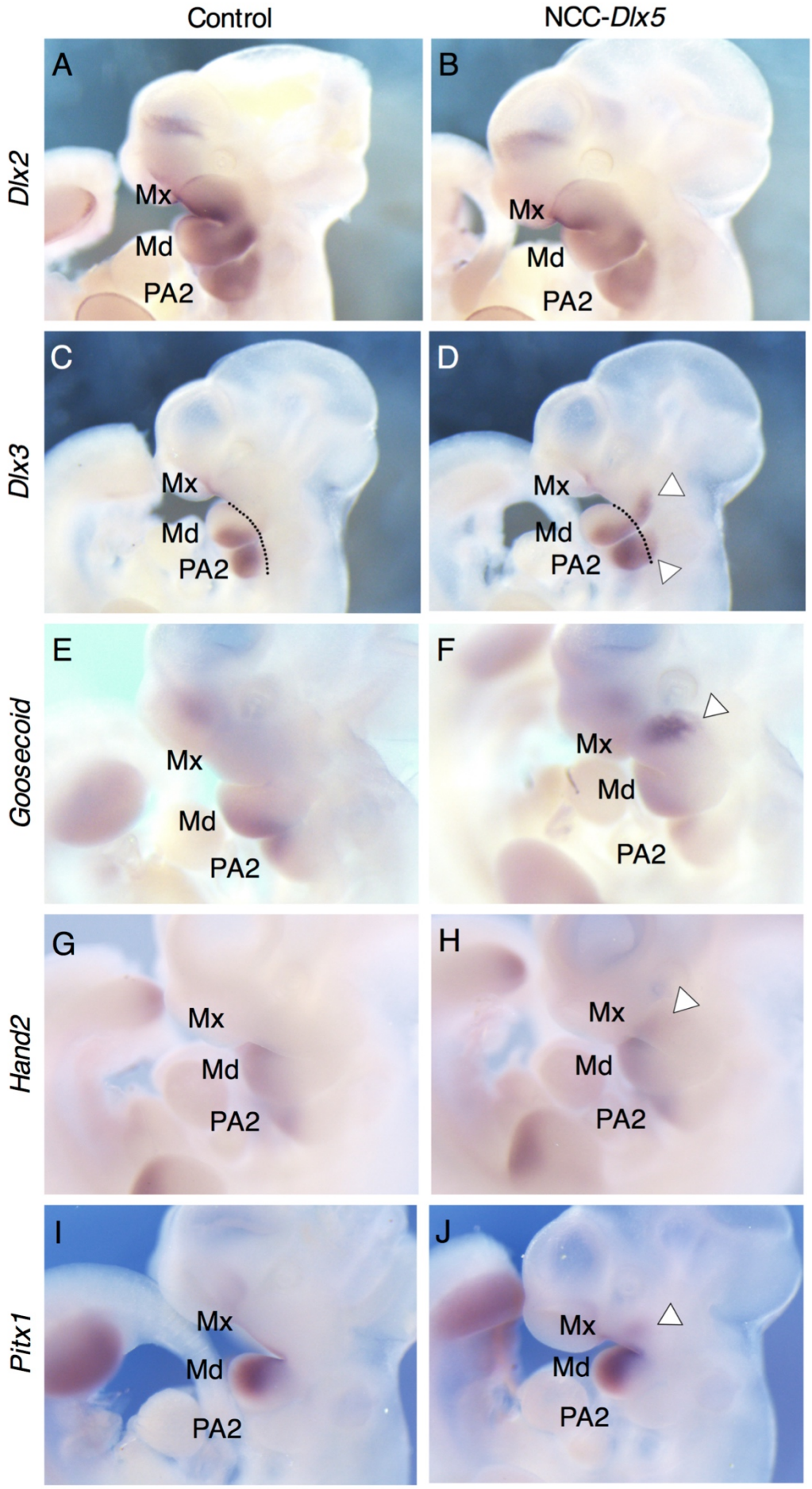
Control
NCC-Dlx5
Dlx2
Dlx3
Goosecoid
Hand2
Pitx1
A
B
C
D
E
F
G
H
I
J
Mx
Md
PA2

Figure 10.

Whole-mount *in situ* hybridization on control and NCC-*Dlx5* embryos.

Whole-mount *in situ* hybridization for *Dlx2* (A and B), *Dlx3* (C and D), *Goosecoid* (E and F), *Hand2* (G and H) and *Pitx1* (I and J) on control and NCC-*Dlx5* embryos at E10.5.

White arrows indicate ectopic expression. Mx, maxillary arch; Md, mandibular arch; PA2, second pharyngeal arch.

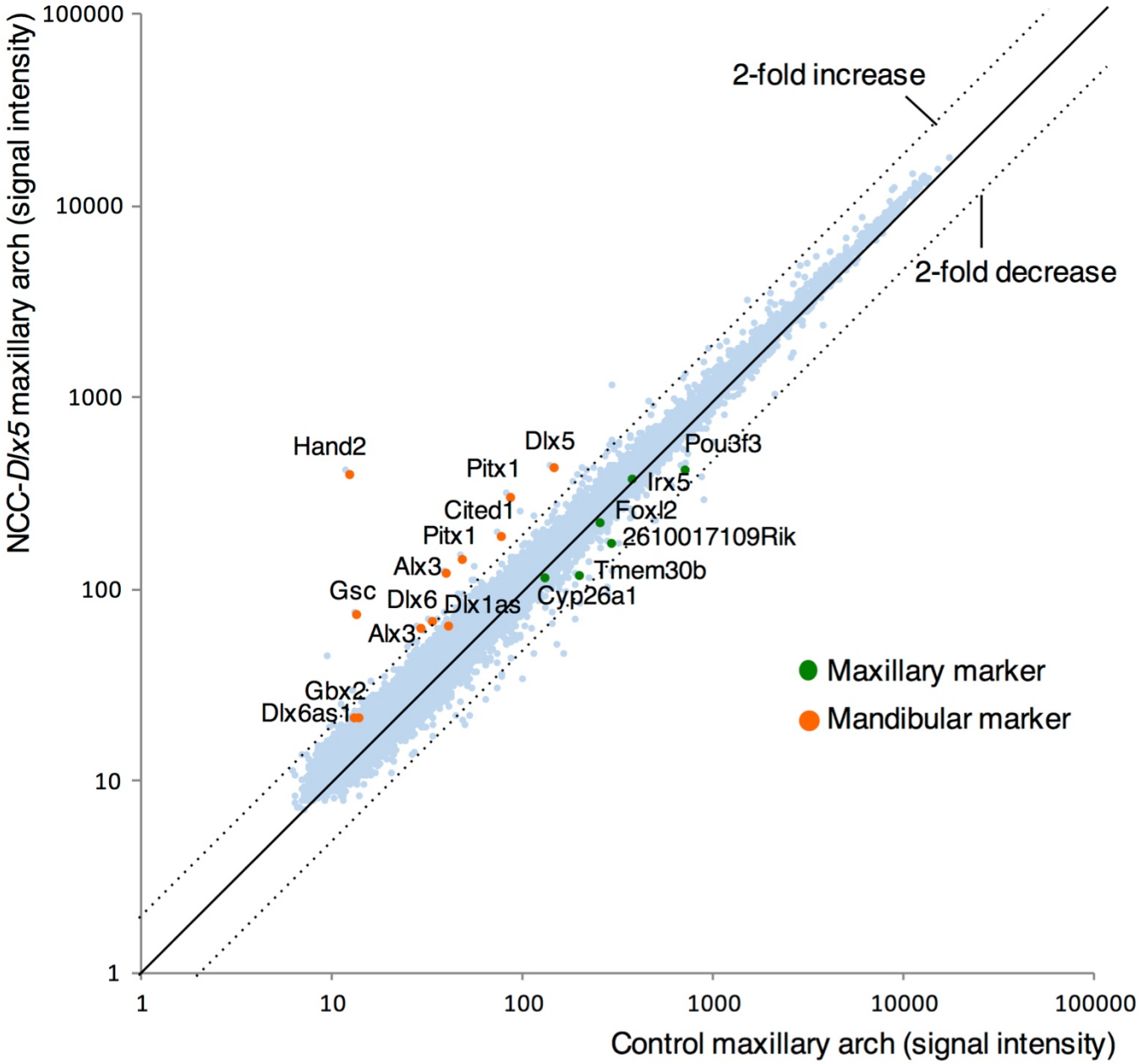

Figure 11.

Scatter plot of signal intensities representing differential gene expression in the E10.5 control and NCC-*Dlx5* maxillary arches.

Plots corresponding to known maxillary and mandibular arch markers are colored green and orange, respectively.

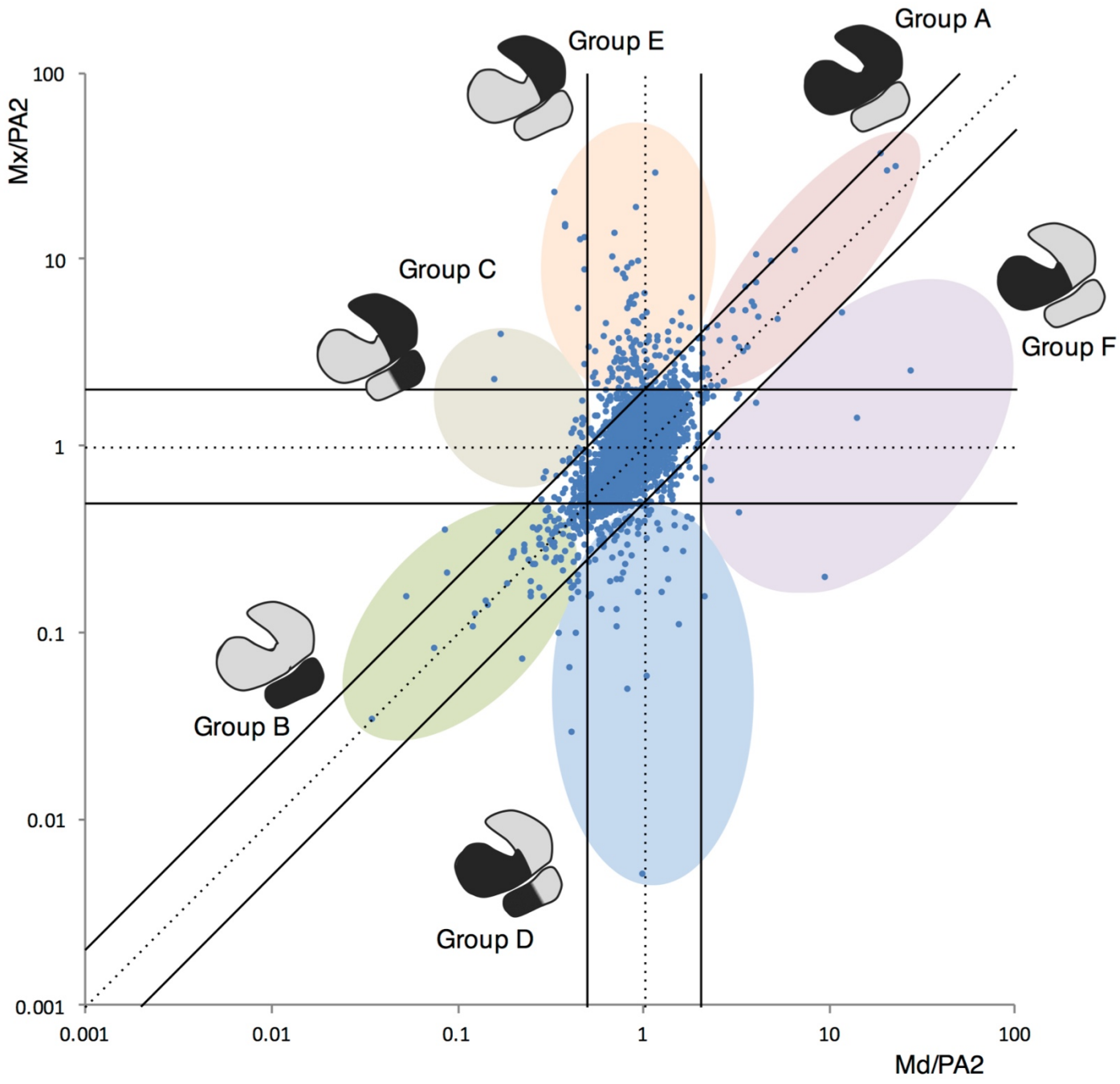

Group A: Anterior (A)-predominant
Group B: Posterior (P)-predominant
Group C: Dorsal (D)-predominant
Group D: Ventral (V)-predominant
Group E: Maxillary (Mx)-predominant
Group F: Mandibular (Md)-predominant

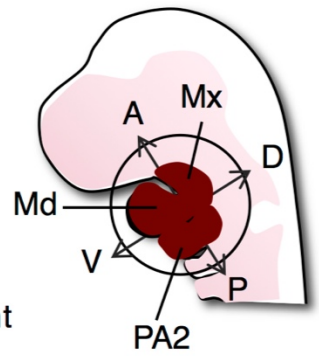

Figure 12.

Diagram for categorization of genes according to expression patterns in PA1 and PA2.

Fold changes of the mandibular arch/PA2 and maxillary arch/PA2 signal intensities from E10.5 control samples were plotted on the abscissa and ordinate, respectively. Based on the plot and previous gene expression data, genes with fold-change difference more than 2 fold between any two of the maxillary arch, mandibular arch and PA2 are categorized into 6 groups as indicated in the diagram with colored zones and schematic expression patterns.

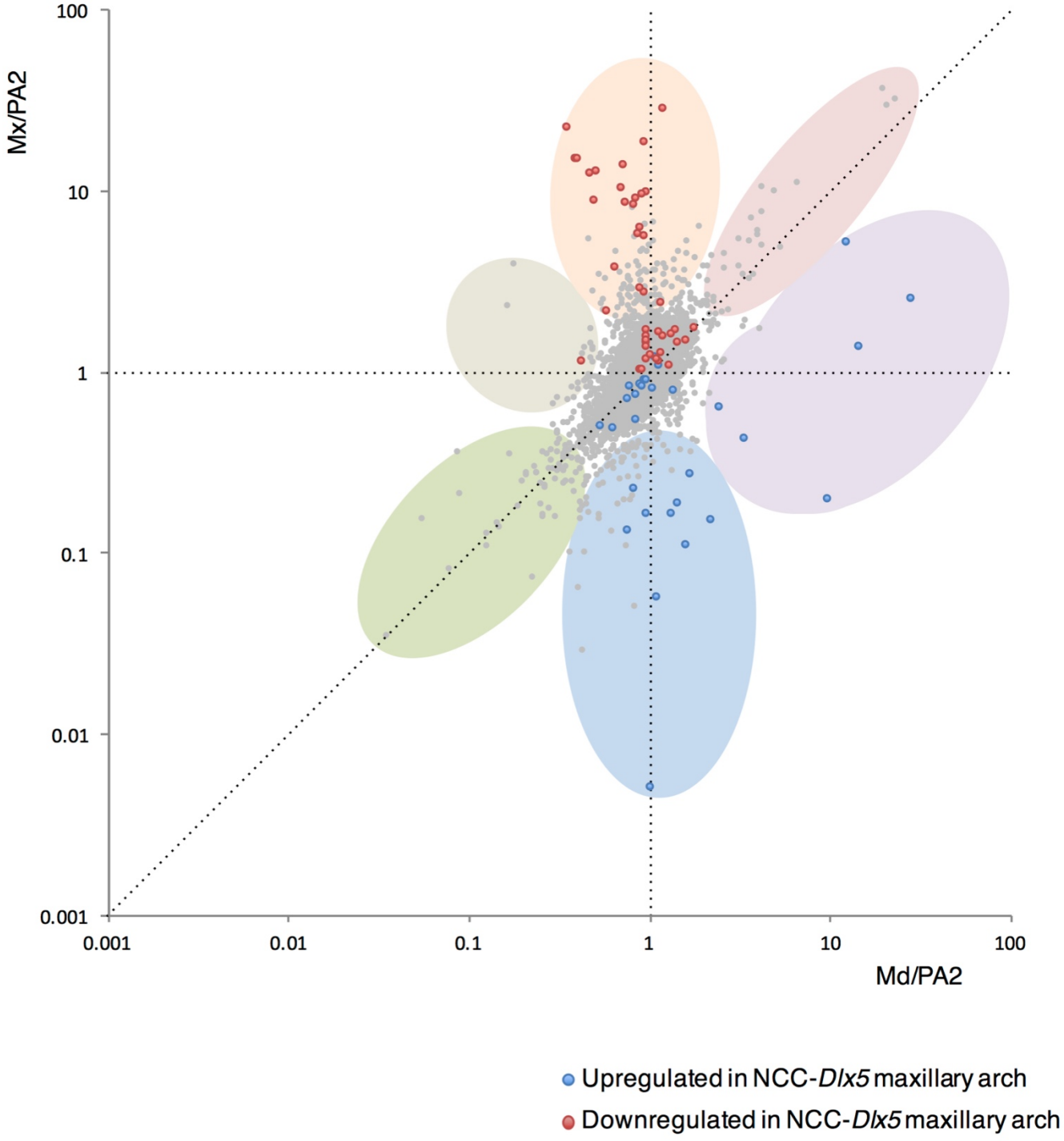

Figure 13.

Categorization of genes upregulated or downregulated in the NCC-*Dlx5* maxillary arch.

Plots corresponding to upregulated or downregulated genes are colored blue or red, respectively.

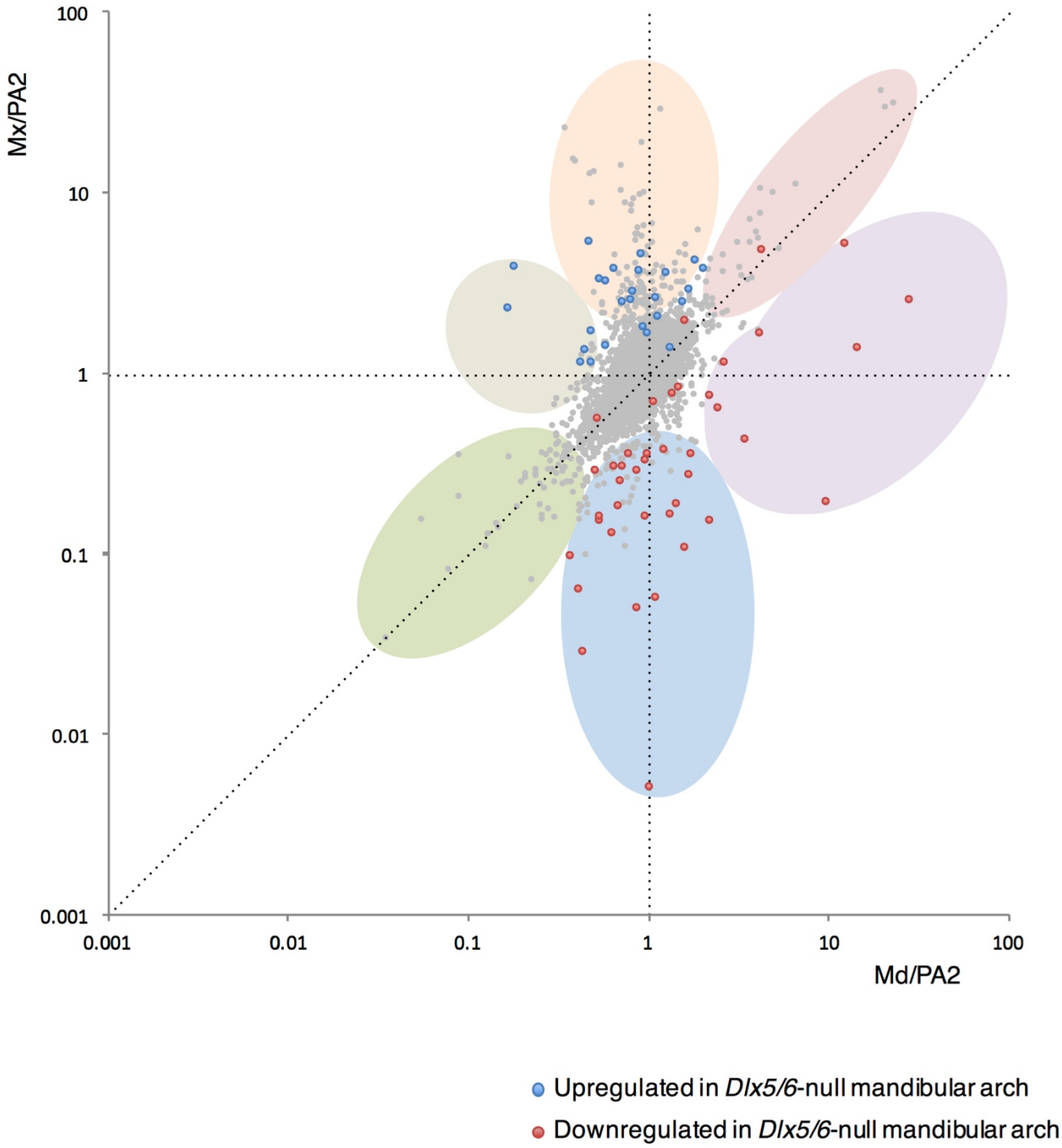

Figure 14.

Categorization of genes upregulated or downregulated in the *Dlx5/6*-null mandibular arch.

Plots corresponding to upregulated or downregulated genes are colored blue or red, respectively.

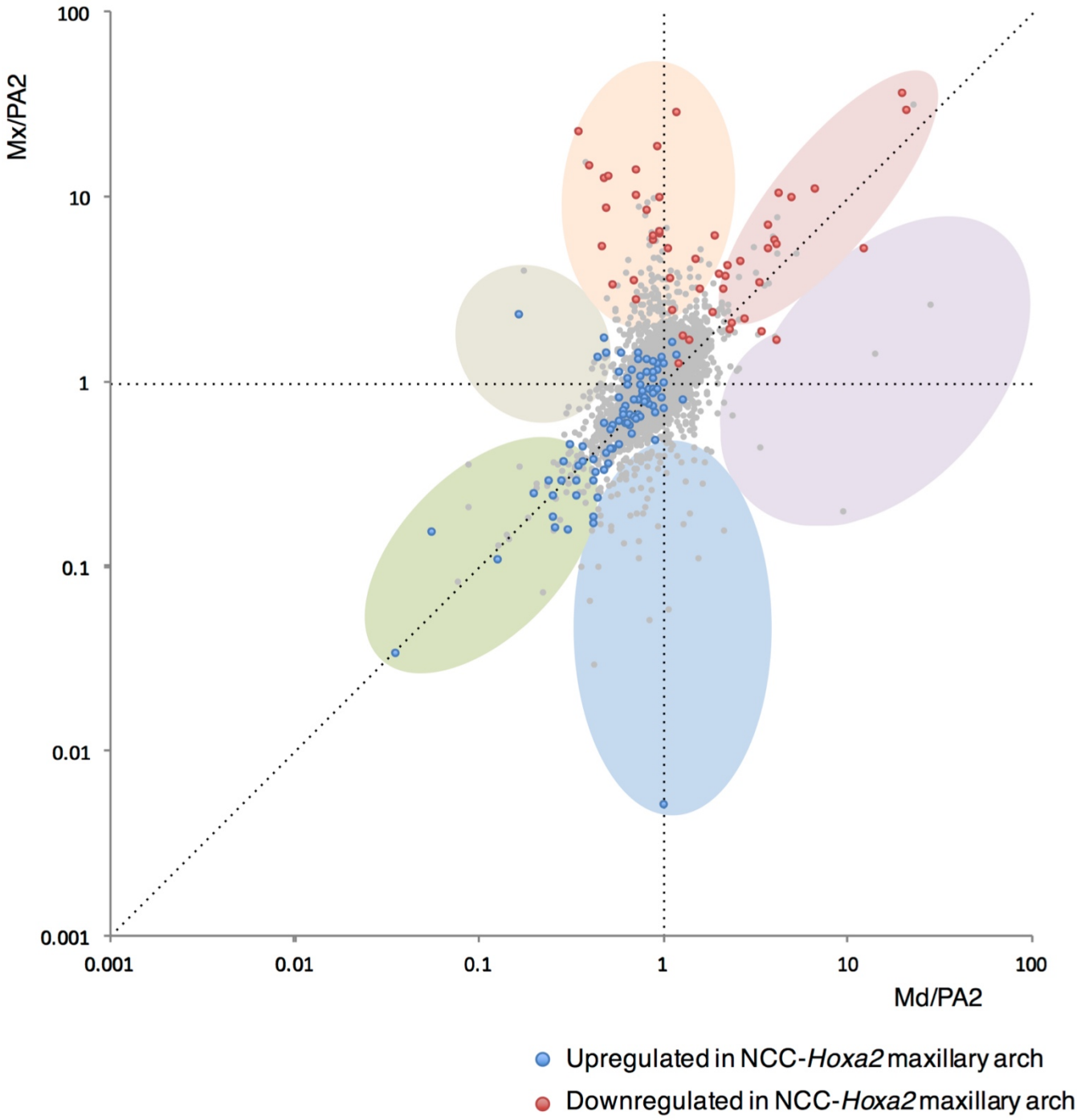

Figure 15.

Categorization of genes upregulated or downregulated in the NCC-*Hoxa2* maxillary arch.

Plots corresponding to upregulated or downregulated genes are colored blue or red, respectively.

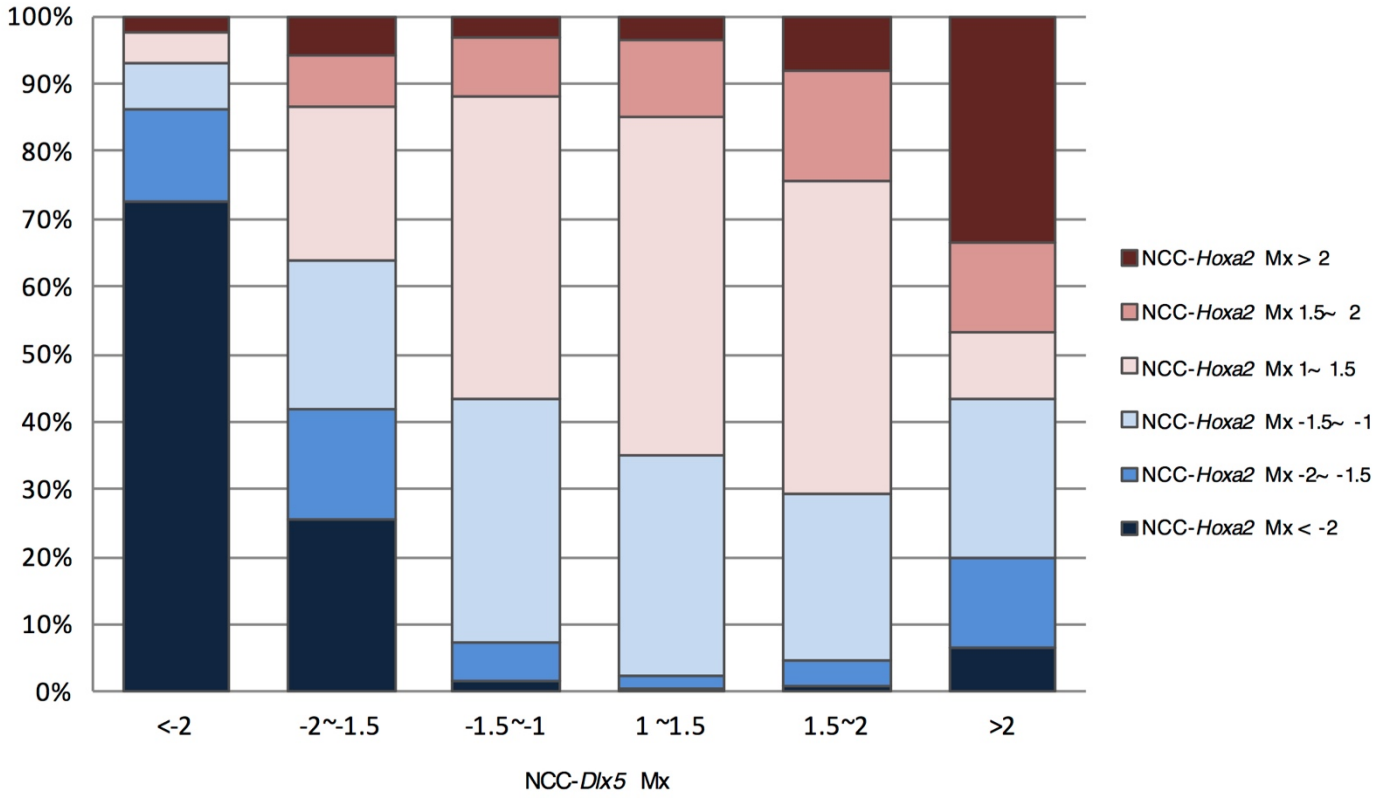

NCC-*Hoxa2* Mx	NCC-*Dlx5* Mx						
	<-2	-2~-1.5	-1.5~-1	1 ~1.5	1.5~2	>2	Total
>2	1	15	418	713	42	10	1199
1.5~2	0	20	1254	2262	83	4	3623
1 ~1.5	2	61	6229	9889	236	3	16420
-1.5~-1	3	58	5054	6404	126	7	11652
-2~-1.5	6	43	761	395	19	4	1228
<-2	32	68	246	79	5	2	432
Total	44	265	13962	19742	511	30	34554

Figure 16.

Stratification analysis based on gene expression profiles of the NCC-*Dlx5* and NCC-*Hoxa2* maxillary arches.

In a horizontal axis, about 35,000 genes are divided into six fractions according to fold difference of expression level between the NCC-*Dlx5* and control maxillary arches at E10.5. Each fraction is further divided into six subfractions according to fold difference between the NCC-*Hoxa2* and control maxillary arches at E10.5. The number of genes in each subfraction is indicated in the table below.

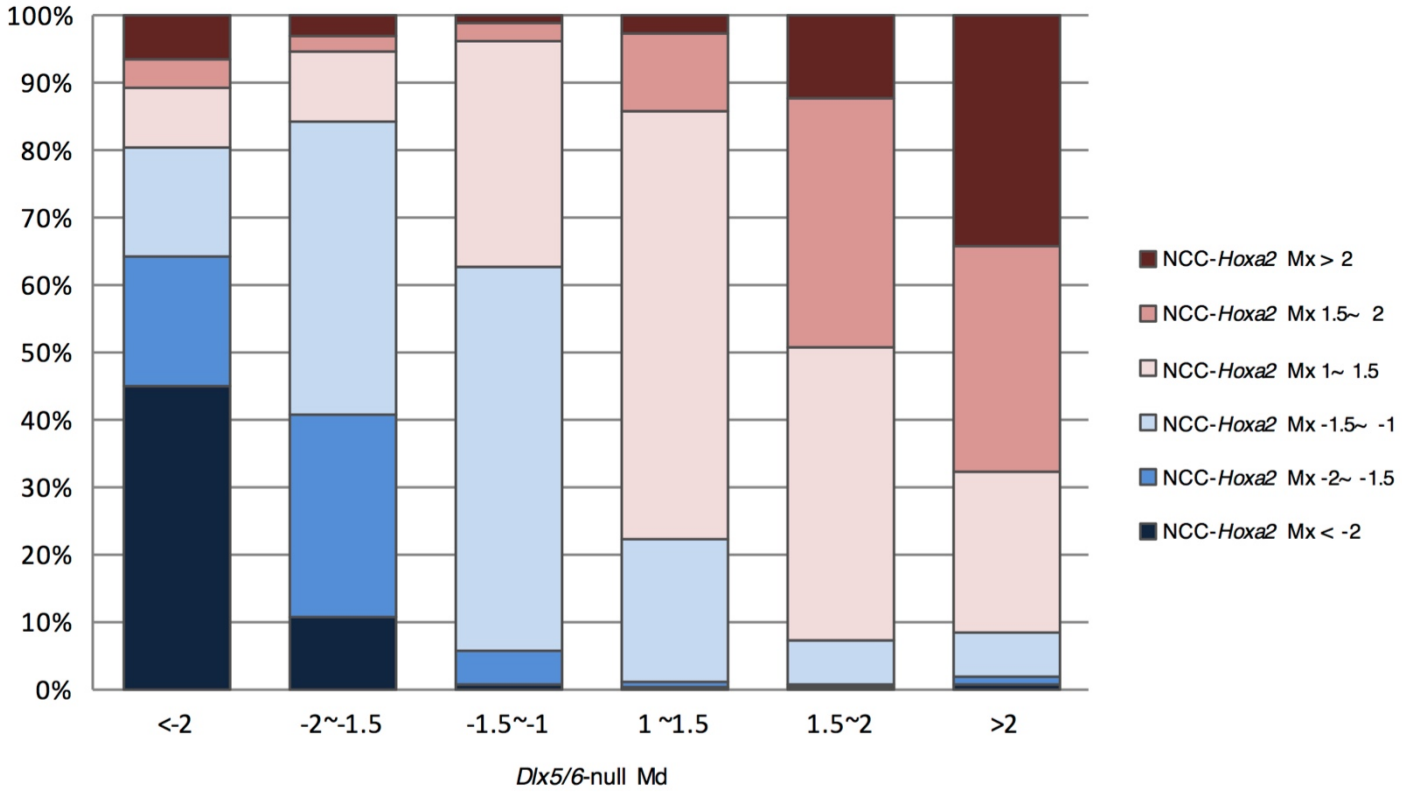

NCC-Hoxa2 Mx	Dlx5/6-null Md						
	<-2	-2~-1.5	-1.5~-1	1 ~1.5	1.5~2	>2	Total
>2	20	35	125	431	360	228	1199
1.5~2	12	27	347	1934	1078	225	3623
1 ~1.5	27	119	4357	10480	1275	162	16420
-1.5~-1	48	495	7366	3515	186	42	11652
-2~-1.5	58	345	672	124	20	9	1228
<-2	136	122	104	58	7	5	432
Total	301	1143	12971	16542	2926	671	34554

Figure 17.

Stratification analysis based on gene expression profiles of the *Dlx5/6*-null mandibular arch and the NCC-*Hoxa2* maxillary arch.

In a horizontal axis, about 35,000 genes are divided into six fractions according to fold difference of expression level between the *Dlx5/6*-null and control mandibular arches at E10.5. Each fraction is further divided into six subfractions according to fold difference between the NCC-*Hoxa2* and control maxillary arches at E10.5. The number of genes in each subfraction is indicated in the table below.

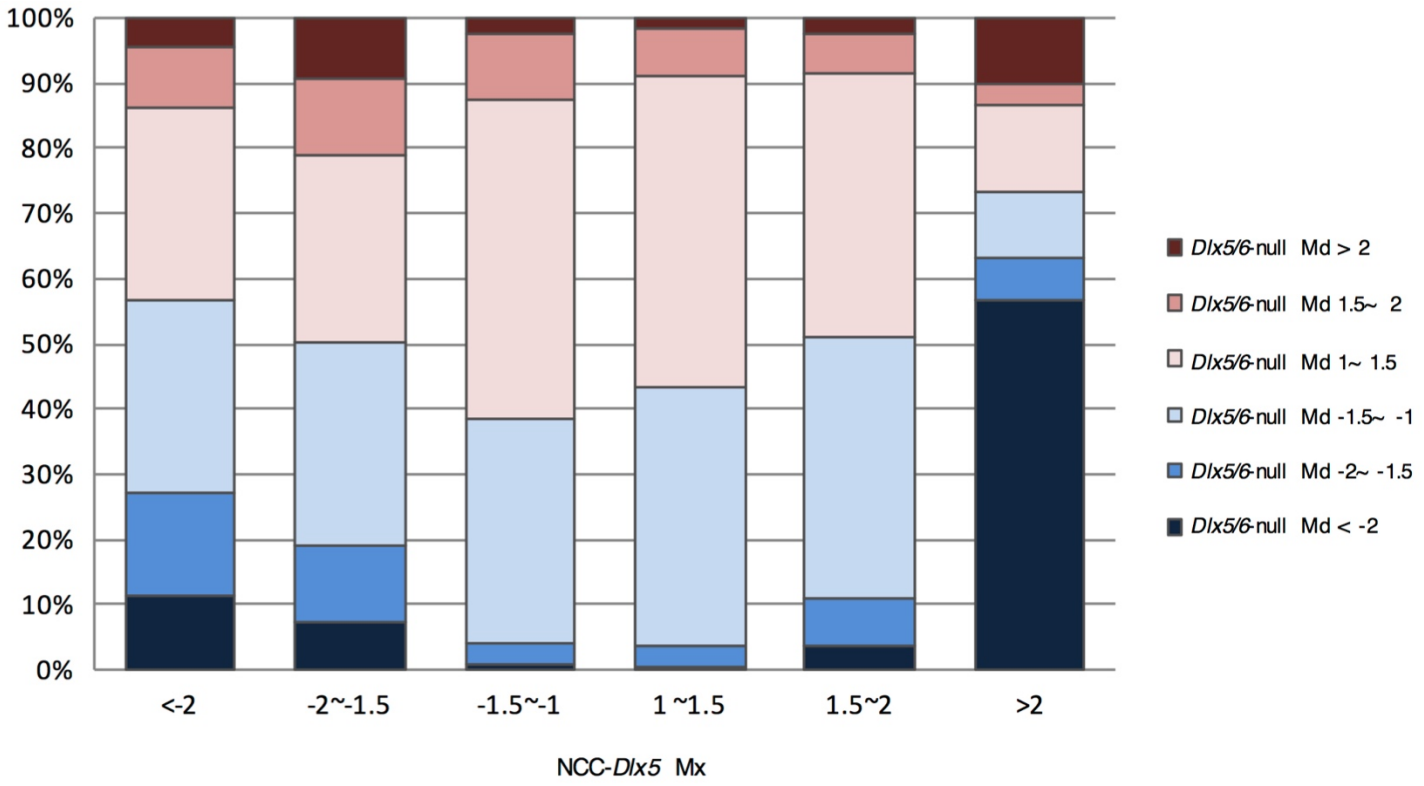

	NCC-*Dlx5* Mx						
Dlx5/6-null Md	<-2	-2~-1.5	-1.5~-1	1 ~1.5	1.5~2	>2	Total
>2	2	25	337	292	12	3	671
1.5~2	4	31	1403	1455	32	1	2926
1 ~1.5	13	76	6836	9406	207	4	16542
-1.5~-1	13	82	4813	7856	204	3	12971
-2~-1.5	7	31	451	614	38	2	1143
<-2	5	20	122	119	18	17	301
Total	44	265	13962	19742	511	30	34554

Figure 18.

Stratification analysis based on gene expression profiles of the NCC-*Dlx5* maxillary arch and the *Dlx5/6*-null mandibular arch.

In a horizontal axis, about 35,000 genes are divided into six fractions according to fold difference of expression level between the NCC-*Dlx5* and control maxillary arches at E10.5. Each fraction is further divided into six subfractions according to fold difference between the *Dlx5/6*-null and control mandibular arches at E10.5. The number of genes in each subfraction is indicated in the table below.

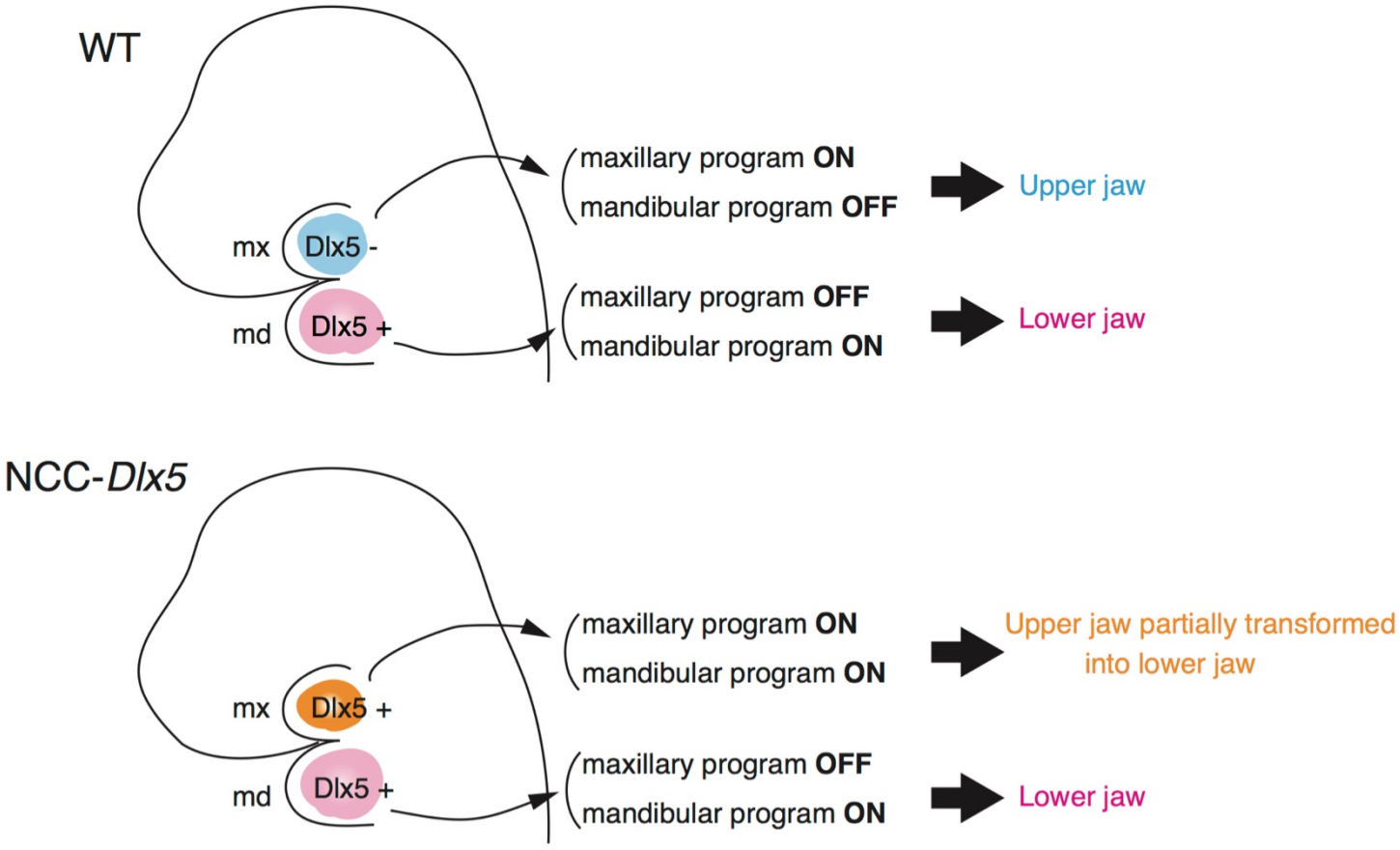

Figure 19.

Scheme illustrating the relationship between *Dlx5* expression and region-specific program in the PA1.

In NCC-*Dlx5* mice, ectopic *Dlx5* induces partial transformation of the upper jaw into a lower jaw-like structure while retaining the upper jaw identity in another part.

Table 1.

Genes upregulated or downregulated in the NCC-*Dlx5* maxillary arch.

Genes upregulated in the NCC-*Dlx5* maxillary arch by more than 2-fold

Affymetrix ID	Gene symbol	Gene name	Chromosome	UniGene	Fold change NCC-*Dlx5* Mx /Control Mx
1436041_at	Hand2	heart and neural crest derivatives expressed 2	chr8	Mm.23651.1	32.4
1421412_at	Gsc	goosecoid	chr12	Mm.129.1	5.4
1455498_at	Gpr50	G-protein-coupled receptor 50	chrX	Mm.33336.1	4.4
1449939_s_at	Dlk1	delta-like 1 homolog (Drosophila)	chr12	Mm.157069.1	3.6
1449488_at	Pitx1	paired-like homeodomain transcription factor 1	chr13	Mm.4832.1	3.5
1459790_x_at	Alx3	aristaless-like homeobox 3	chr3	Mm.141865.1	3.0
(1419514_at	Pitx1	paired-like homeodomain transcription factor 1	chr13	Mm.4832.1	3.0)
1449863_a_at	Dlx5	distal-less homeobox 5	chr6	Mm.4873.1	2.9
1449031_at	Cited1	Cbp/p300-interacting transactivator with Glu/Asp-rich carboxy-terminal domain 1	chrX	Mm.2390.1	2.5
1419152_at	2810417H13Rik	RIKEN cDNA 2810417H13 gene	chr9	Mm.45765.1	2.4
1438586_at	Tbx22	T-box 22	chrX	Mm.137011.1	2.2
1420143_at	Rc3h2	ring finger and CCCH-type zinc finger domains 2	chr2	Mm.36240.2	2.2
(1420555_at	Alx3	aristaless-like homeobox 3	chr3	Mm.10112.1	2.1)
1452507_at	Dlx6	distal-less homeobox 6	chr6	Mm.5152.1	2.0

Genes downregulated in the NCC-*Dlx5* maxillary arch by more than 2-fold

Affymetrix ID	Gene symbol	Gene name	Chromosome	UniGene	Fold change NCC-*Dlx5* Mx /Control Mx
1426255_at	Nefl	neurofilament, light polypeptide	chr14	Mm.1956.1	-3.3
1417954_at	Sst	somatostatin	chr16	Mm.2453.1	-3.1
1426412_at	Neurod1	neurogenic differentiation 1	chr2	Mm.4636.1	-2.9
(1426413_at	Neurod1	neurogenic differentiation 1	chr2	Mm.4636.1	-2.9)
1429668_at	Pou4f1	POU domain, class 4, transcription factor 1	chr14	Mm.132990.1	-2.8
1438511_a_at	Rgcc	regulator of cell cycle	chr14	Mm.29811.2	-2.7
(1454672_at	Nefl	neurofilament, light polypeptide	chr14	Mm.41752.1	-2.6)
1436994_a_at	Hist1h1c	histone cluster 1, H1c	chr13	Mm.193539.5	-2.6
1455865_at	Insm1	insulinoma-associated 1	chr2	Mm.77063.1	-2.6
1423281_at	Stmn2	stathmin-like 2	chr3	Mm.29580.1	-2.6
1448991_a_at	Ina	internexin neuronal intermediate filament protein, alpha	chr19	Mm.2496.1	-2.5
1422520_at	Nefm	neurofilament, medium polypeptide	chr14	Mm.142140.1	-2.4
1415978_at	Tubb3	tubulin, beta 3 class III	chr8	Mm.40068.1	-2.4
1452894_at	Elavl4	ELAV (embryonic lethal, abnormal vision, Drosophila)-like 4 (Hu antigen D)	chr4	Mm.3970.3	-2.4
1418678_at	Has2	hyaluronan synthase 2	chr15	Mm.5148.1	-2.3
1438551_at	Neurog1	neurogenin 1	chr13	Mm.57230.2	-2.3
1450779_at	Fabp7	fatty acid binding protein 7, brain	chr10	Mm.3644.1	-2.3
1442786_s_at	Rufy3	RUN and FYVE domain containing 3	chr5	Mm.195906.1	-2.2
1438069_a_at	Rbm5	RNA binding motif protein 5	chr9	Mm.46706.2	-2.1
(1423280_at	Stmn2	stathmin-like 2	chr3	Mm.29580.1	-2.1)
1457086_at	D930028M14Rik	RIKEN cDNA D930028M14 gene	chr7	Mm.59171.1	-2.1
1444980_at	Onecut2	one cut domain, family member 2	chr18	Mm.153232.1	-2.0
1456712_at	Lcorl	ligand dependent nuclear receptor corepressor-like	chr5	Mm.71593.1	-2.0
1431096_at	Ints8	integrator complex subunit 8	chr4	Mm.158856.1	-2.0
(1429667_at	Pou4f1	POU domain, class 4, transcription factor 1	chr14	Mm.132990.1	-2.0)

Table 2.

Comparison of genes affected in the NCC-*Dlx5* maxillary arch and those affected in the *Dlx5/6*-null mandibular arch.

NCC-*Dlx5* Mx/Control Mx		*Dlx5/6*-null Md/Control Md	
Up	Down	Up	Down
Hand2	Nefl	Pou3f3	Dlx5
Gsc	Sst	Tmem30b	Dlx6
Gpr50	Neurod1	2900092D14Rik	Dlx6os1
Dlk1	Pou4f1	Itih5	Dlx1as
Pitx1	Rgcc	B230214O09Rik	Gm2818
Alx3	Hist1h1c	Bdnf	Gsc
Dlx5	Insm1	Foxl2	Hand2
Cited1	Stmn2	Foxl2os	Gpr50
2810417H13Rik	Ina	2610017I09Rik	Tbx22
Tbx22	Nefm	Igf1	Gbx2
Rc3h2	Tubb3	Cyp26a1	Pitx1
Dlx6	Elavl4	Crym	Dgkk
	Has2	Has2	Col8a2
	Neurog1	Six1	Alx3
	Fabp7	Mtap2	Dkk2
	Rufy3	Ptx3	Sdpr
	Rbm5	Figf	Dlx6os2
	D930028M14Rik	Ebf2	Rgs5
	Onecut2		Dlx4
	Lcorl		Cited1
	Ints8		Lrrc17
			Zadh2
			Shox2
			Aldh1a2
			Osr1
			Ptprz1
			Tshz1
			Dlk1
			Pcdh19
			Gm6958
			Nr5a2
			Tnnt1
			Nrk
			A730090H04Rik
			9430047L24Rik
			Pmp22
			A130040M12Rik
			Rspo2
			Arg2
			Synpo2
			Pdgfrl
			Bmper
			1110006E14Rik
			Plcxd3
			Hist3h2ba

Overlapping genes are colored correspondingly.

Table 3.

Characterization of genes upregulated or downregulated in both the NCC-*Dlx5* and NCC-*Hoxa2* maxillary arches.

Genes upregulated in both the NCC-*Dlx5* and NCC-*Hoxa2* maxillary arches by more than 2-fold

Gene symbol	GO biological process
Hand2	cartilage morphogenesis, heart development, negative regulation of osteoblast differentiation, negative regulation of apoptotic process
Cited1	negative regulation of osteoblast differentiation, negative regulation of neuron apoptotic process, embryonic axis specification
Dlx5	bone morphogenesis, ear development, face morphogenesis, ossification, axon guidance, head development, palate development, positive regulation of osteoblast differentiation
Igfbp5	negative regulation of osteoblast differentiation, negative regulation of cell migration
Bnc1	chromosome organization, positive regulation of epithelial cell proliferation, regulation of transcription from RNA polymerase I promoter, regulation of transcription from RNA polymerase II promoter
Dlx1as	embryonic cranial skeleton morphogenesis
Rpl27a	translation
Dlx6	embryonic limb development, head development, inner ear morphogenesis, palate development
Unc5c	brain development, anterior/ posterior axon guidance, regulation of cell migration
Hist1h3b	DNA replication-dependent nucleosome assembly, nucleosome assembly, positive regulation of defense response to virus by host

Genes upregulated in the NCC-*Dlx5* maxillary arch and downregulated in the NCC-*Hoxa2* maxillary arch by more than 2-fold

Gene symbol	GO biological process
Dlk1	cell differentiation, embryonic skeletal development, negative regulation of Notch signaling pathway, regulation of gene expression
Tbx22	negative regulation of transcription

Genes downregulated in both the NCC-*Dlx5* and NCC-*Hoxa2* maxillary arches by more than 2-fold

Gene symbol	GO biological process
Nefl	neuron projection morphogenesis, negative regulation of neuron apoptotic process
Neurod1	neuron, cerebellum, dentate gyrus, hindbrain & inner ear development,
Sst	cell surface receptor signaling pathway, cell-cell signaling, regulation of cell migration
Eif2s3y	translation initiation
Insm1	nervous system development, noradrenergic neuron development, positive regulation of cell cycle arrest/ cell differentiation/ cell migration, cell proliferation
Tubb3	axon guidance, neuron differentiation
Nefm	neurofilament cytoskeleton organization, microtubule cytoskeleton organization
Kdm5d	chromatin modification, histon H3-K4 demethylation
Stmn2	positive & negative regulation of neuron projection development
Elavl4	dendrite morphogenesis, neuron differentiation, learning, locomotory behavior
Ina	cell differentiationm nervous system development, neurofilament cytoskeleton organization
Neurog1	neuron differentiation, nervous system development, inner ear morphogenesis
Ppp1r17	negative regulation of catalytic activity, regulation of phosphatase activity
Pou4f1	negative regulation of neuron apoptotic process, neuron differentiation, neuron fate specification, peripheral nervous system neuron development
Rab11fip5	protein transport, regulated secretory pathway
Rgcc	negative regulation of angiogenesis/ cell proliferation/ exit from mitosis, positive regulation of cell cycle arrest, positive regulation fo cytokine secration
Fabp7	neurogenesis, cell proliferation in forebrain, epithelial cell proliferation
Ganab	N-glucan processing, carbohydrate metabolic process, metabolic process
Ntrk2	nervius system development, neuromuscular junction development, long-term memory
Tmsb10	actin cytoskeleton organization
Abcf1	positive regulation of translation, translation initiation
Rufy3	nervous system development, positive regulation of axon extention/ axonogenesis/ cell migration
Pdilt	cell differentiation, cell migration, spermatid development, apermatogenesis
Gm19310	(unknown)
Lrrc4	synapse organization, negative regulation of JAK-STAT cascade/ protein kinase activity
Per3	circadian regulation of gene expression, circadian rhythm
Skap1	immune system process, adaptive immune response, positive regulation of cell adhesion
Nhlh2	cell differentiation, mating behavior, ovulation cycle
4930425F17Rik	(unknown)

Genes downregulated in the NCC-*Dlx5* maxillary arch and upregulated in the NCC-*Hoxa2* maxillary arch by more than 2-fold

Gene symbol	GO biological process
Has2	bone morphogenesis, positive regulation of cell migration/ cell proliferation

Table 4.

Characterization of Hoxa2-bound genes affected by Dlx5.

Genes upregulated in the NCC-*Dlx5* maxillary arch by more than 2-fold

Gene symbol	GO biological process	Fold change	
		NCC-*Dlx5* Mx /Control Mx	NCC-*Hoxa2* Mx /Control Mx
Dlk1	cell differentiation, embryonic skeletal development, negative regulation of Notch signaling pathway, regulation of gene expression	3.9	−2.9

Genes downregulated in the NCC-*Dlx5* maxillary arch by more than 2-fold

Gene symbol	GO biological process	Fold change	
		NCC-*Dlx5* Mx /Control Mx	NCC-*Hoxa2* Mx /Control Mx
Nefl	neuron projection morphogenesis, negative regulation of neuron apoptotic process	−4.4	−17.0
Stmn2	positive & negative regulation of neuron projection development	−2.8	−8.3

Genes upregulated in the *Dlx5/6*-null mandibular arch by more than 2-fold

Gene symbol	GO biological process	Fold change	
		Dlx5/6−null Md /Control Md	NCC-*Hoxa2* Md /Control Md
Map2	central nervous system neuron development, dendrite development, establishment of cell polarity, regulation of axonogenesis	3.6	1.0
Cyp26a1	anterior/posterior pattern specification, central nervous system development, neural crest cell development, retinoic acid catabolic process	3.6	5.8
Adamts9	positive regulation of melanocyte differentiation, regulation of developmental pigmentation, proteolysis	3.6	1.5
Angpt1	in utero embryonic development, angiogenesis, negative regulation of apoptotic process, cardiac muscle tissue morphogenesis	3.5	1.8
Ptx3	innate immune response, negative regulation by host of viral exo-alpha-sialidase activity, positive regulation of nitric oxide biosynthetic process	3.5	1.8
Bdnf	inner ear development, negative regulation of apoptotic process, negative regulation of neuroblast proliferation	3.3	−1.2
Lepr	G-protein coupled receptor signaling pathway, angiogenesis, positive regulation of MAPK cascade	3.0	3.4
Rspo3	positive regulation of canonical Wnt signaling pathway, angiogenesis, branching involved in labyrinthine layer morphogenesis	2.6	−1.6
Prickle1	negative regulation of canonical Wnt signaling pathway, negative regulation of cardiac muscle cell myoblast differentiation, neural tube closure	2.5	1.5
Fzd4	G-protein coupled receptor signaling pathway, Wnt signaling, blood vessel development	2.4	6.5
Sema3e	negative regulation of angiogenesis, nervous system development, positive regulation of cell migration	2.4	2.5
Mafb	brain segmentation, inner ear mirphogenesis, negative regulation of osteoclast differentiation	2.3	3.5
Six1	embryonic cranial skeleton morphogenesis, embryonic skeletal system morphogenesis, facial nerve morphogenesis, inner ear development	2.1	−2.4
Fibin	(unknown)	2.1	2.8
Flrt2	heart morphogenesis, fibroblast growth factor receptor signaling pathway, basement membrane organization	2.1	1.8
Cbln1	cerebellar granule cell differentiation, heterophilic cell-cell adhesion via plasma membrane cell adhesion molecules, positive regulation of synapse assembly	2.0	3.4

Genes downregulated in the *Dlx5/6*-null mandibular arch by more than 2-fold

Gene symbol	GO biological process	Fold change	
		Dlx5/6−null Md /Control Md	NCC-*Hoxa2* Md /Control Md
Dlx6as1	positive regulation of transcription from RNA polymerase II promoter	−21.5	12.4
Dlk1	cell differentiation, embryonic skeletal development, negative regulation of Notch signaling pathway, regulation of gene expression	−4.8	−2.9
Osr1	embryonic skeletal joint morphogenesis, embryonic forelimb morphogenesis, embryonic hindlimb morphogenesis, heart development	−3.2	−1.4
Barx1	anterior/posterior pattern specification, digestive system development, negative regulation of Wnt signaling pathway	−2.8	−4.0
Nr5a2	positive regulation of transcription from RNA polymerase II promoter, epithelial cell differentiation, regulation of cell proliferation	−2.8	−1.0
Msx1	face morphogenesis, bone morphogenesis, cartilage morphogenesis, epithelial to mesenchymal transition, embryonic forelimb morphogenesis, embryonic hindlimb morphogenesis	−2.6	−3.2
Msc	branchiomeric skeletal muscle development, palate development, negative regulation of transcription from RNA polymerase II promoter	−2.3	−1.0
Runx1t1	regulation of transcription, fat cell differentiation, regulation of DNA binding	−2.1	2.3
Rspo2	positive regulation of canonical Wnt signaling pathway, bone mineralization, osteoblast differentiation, embryonic forelimb morphogenesis, embryonic hindlimb morphogenesis	−2.1	−2.9
Shox2	cartilage development involved in endochondral bone morphogenesis, chondrocyte development, osteoblast differentiation, muscle tissue morphogenesis	−2.0	−1.3